The 2nd Tsukuba Workshop on Ferroelectrics (TWF-2)

Abstract Book

Nov. 14 (Mon), 2005

Laboratory of Advanced Research B, University of Tsukuba
Tsukuba, Ibaraki 305-8573, Japan

TWF-2 Access Guide

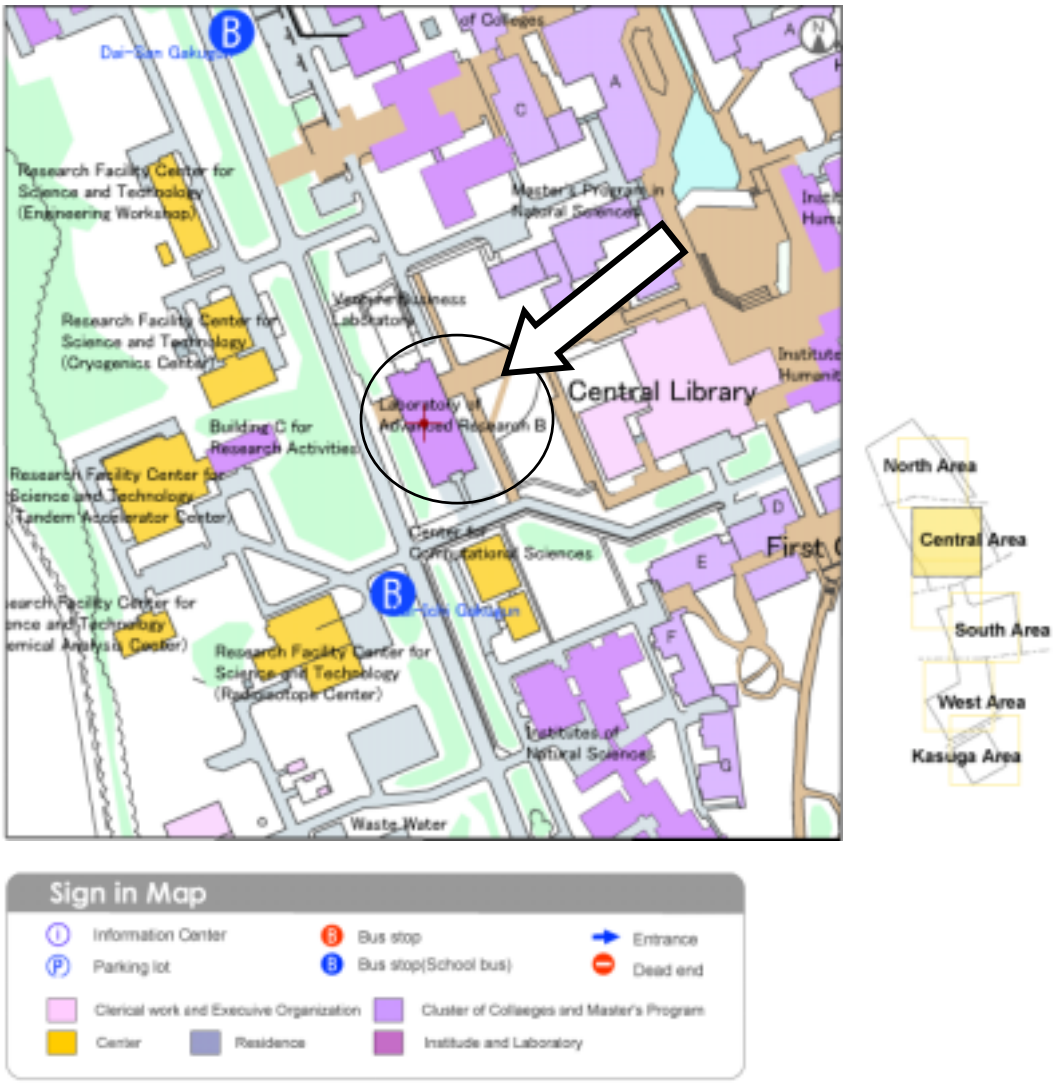

Lectures will be in the 0108 presentation room of the Laboratory of Advanced Research B (First Floor).

Traffic Routes to University of Tsukuba (Tsukuba area)

If you need detailed train information or timetable, please refer to the following URL.
http://www.tsukuba.ac.jp/eng/navi/access.html

Workshop Program

13:25-13:30 Opening address S. Kojima (IMS, Univ. of Tsukuba)

13:30-14:00 "Quasi-elastic light scattering of the relaxor ferroelectrics"
S. Lushnikov (Ioffe. Institute. Russia)……...**4**

14:00-14:30 "Non-ergodic behavior of polar state in Li-doped $KTaO_3$ under electric field"
Y. Uesu (Waseda University)……**5**

14:30-15:00 "Spectroscopic observation of bipolaronic point defects and small-polaron excitations in $Ba_{1-x}K_xBiO_3$"
H. Uwe (IMS, Univ. of Tsukuba)……**12**

15:00-15:10 Coffee break

15:10-15:40 "Phase transition in Bi-layered perovskite and a model of ultra-thin ferroelectric film"
A. Onodera (Hokkaido University)…….**16**

15:40-16:10 "Universality of the lead-free piezoelectric solid solution (Na,K) NbO_3-$ATiO_3$"
R. Wang (AIST)……..**18**

16:10-16:40 "Ferroelectric domain structures near the MPB of $Pb(Zr_{1-x}Ti_x)O_3$"
T. Asada (Waseda University)…….**20**

16:40-17:00 "Order-disorder nature of ferroelectric $BaTi_2O_5$"
H. Anwar (IMS, Univ. of Tsukuba)…….**22**

17:00-17:20 "Microheterogeneity and field-cooling effects on $Pb[(Zn_{1/3}Nb_{2/3})_{0.955}Ti_{0.045}]O_3$ single crystals probed by micro-Brillouin scattering"
D.H. Kim (IMS, Univ. of Tsukuba)……**26**

17:20-17:40 "Vibrational Properties of Protein"

A. Svanidze (Ioffe. Institute. Russia)……..**30**

17:40 Closing

18:00- Banquet (Lamp)

Quasi-elastic light scattering in relaxor ferroelectrics

Sergey LUSHNIKOV

A.F. Ioffe Physical Technical Institute of RAS, 194021, St.Petersburg, Russia
e-mail: sergey.lushnikov@mail.ioffe.ru

In my report results of studying of $PbMg_{1/3}Nb_{2/3}O_3$ (PMN), $PbMg_{1/3}Ta_{2/3}O_3$ (PMT), $PbSc_{1/2}Ta_{1/2}O_3$ (PST), and $Na_{1/2}Bi_{1/2}TiO_3$ (NBT) and KNSBN:Cu crystals by micro–Brillouin light scattering are presented. Need to note, that PMN, PMT, PST and NBT crystals are cubic relaxor ferroelectrics while KNSBN is a uniaxial relaxor crystal with tungsten bronze structure. It is clearly seen in temperature behavior of the low-frequency vibration spectra: the velocity anomaly and corresponding broad maximum of damping in relaxors well correlate with the main dielectric maximum in the vicinity of a diffuse phase transition. The anomalies are absent in BMT crystals where the acoustic response is determined by anharmonicity. Unusual frequency dispersion of the longitudinal acoustic phonons (LA) in PMN and PMT crystals was observed in our experiments. Investigation of the Brillouin scattering by Sandercock's tandem system gives possibility for correct analysis of the low frequency part of the vibration spectra of the crystals. We observed quasi-elastic light scattering and separated this addition contribution from the scattering spectra of the studied crystals vs temperature. It was found that quasi-elastic light scattering in relaxors has a complicate structure and temperature behaviour.

Presence of the quasi-elastic scattering with such properties (relaxation mode) shows that despite previous expectations order-disorder behaviour plays an important role in the dynamics of the diffuse phase transition.

In present report I would like to discuss: *(1)* Our new results of neutron and light scattering studies *(2)* Relation of our observation with previously published neutron and light scattering data.

Non-ergodic behavior of polar state in Li-doped $KTaO_3$ under an electric field

Hiroko YOKOTA, Taeko OYAMA, and Yoshiaki UESU

Department of Physics, Waseda University

Incipient ferroelectric $KTaO_3$ with off-center Li impurity of the critical concentration of 2.8 mol% was investigated in order to clarify the dipole state under electric field. Using optical second-harmonic generation (SHG) microscope, we observed a marked history dependence of SHG intensity through zero-field cooling (ZFC), zero-field heating (ZFH), field heating after ZFC (FH/ZFC) and FH after field cooling (FH/FC). These show different paths with respect to temperature: In the ZFC/ZFH process, weak SHG was observed at low temperature, while in the FH/ZFC process, relatively high SHG appears in a limited temperature range below T_F depending on the field strength, and in the FC and FH/FC processes, the SHG exhibits ferroelectric-like temperature dependence: it appears at the freezing temperature of 50K, increases with decreasing temperature and has a tendency of saturation. These experimental results strongly suggest that dipole glass state or polar nano-clusters which gradually freezes with decreasing temperature is transformed into semi-macroscopic polar state under the electric field. However at sufficiently low temperature, the freezing is so strong that the electric field cannot enlarge the polar clusters. These experimental results show that the polar nano-cluster model similar to relaxors would be more relevant in $KTaO_3$ doped with the critical concentration of Li. Further experiments on the anisotropy of SHG determine that the average symmetry of the field-induced polar phase is tetragonal 4mm or 4. The tetragonality is also confirmed by the X-ray diffraction measurement.

Second-harmonic-generation microscopic observations of polar state in Li-doped $KTaO_3$ under an electric field

Hiroko Yokota,* Taeko Oyama, and Yoshiaki Uesu
Department of Physics, Waseda University, 3-4-1 Okubo, Shinjuku-ku, Tokyo 169-8555, Japan
(Received 24 June 2005; revised manuscript received 5 August 2005; published 7 October 2005)

Incipient ferroelectric $KTaO_3$ with off-center Li impurity of the critical concentration of 2.8 mol % was investigated in order to clarify the dipole state under electric field. Using optical second-harmonic generation (SHG) microscope, we observed a marked history dependence of SHG intensity through zero-field cooling (ZFC), zero-field heating (ZFH), field heating after ZFC (FH/ZFC), and FH after field cooling (FH/FC). These show different paths with respect to temperature: In the ZFC/ZFH process, weak SHG was observed at low temperature, while in the FH/ZFC process, relatively high SHG appears in a limited temperature range below T_F depending on the field strength, and in the FC and FH/FC processes, the SHG exhibits ferroelectriclike temperature dependence: it appears at the freezing temperature of 50 K, increases with decreasing temperature, and has a tendency of saturation. These experimental results strongly suggest that dipole glass state or polar nanoclusters which gradually freezes with decreasing temperature is transformed into a semimacroscopic polar state under the electric field. However at sufficiently low temperature, the freezing is so strong that the electric field cannot enlarge the polar clusters. These experimental results show that the polar nanocluster model similar to relaxors would be more relevant in $KTaO_3$ doped with the critical concentration of Li. Further experiments on the anisotropy of SHG determine that the average symmetry of the field-induced polar phase is tetragonal 4 mm or 4. The tetragonality is also confirmed by the x-ray diffraction measurement.

DOI: 10.1103/PhysRevB.72.144103 PACS number(s): 61.50.Ks, 61.72.Ww, 64.70.Kb, 42.65.Ky

I. INTRODUCTION

$KTaO_3$ is known to be one of the representatives of quantum paraelectrics.[1–4] The quantum paraelectricity is a characteristic feature exhibited by several anharmonic optical phonon systems.[5] Due to self-energy, the frequency of the lowest lying optical mode becomes strongly temperature dependent with general tendency that the frequency becomes remarkably reduced as $T \rightarrow 0$ K, which is called soft optic mode. With the renormalization due to the quartic anharmonicity, there exists a finite temperature T_0, where the soft phonon frequency equals to zero and the high temperature phase becomes instable. Actually, however, at low temperature, the quantum fluctuations (zero point vibration) start to play a role to tend to suppress the instability. When the renormalization effect is sufficiently large, the lattice stays on cubic down to $T=0$ K. Such a system is called quantum paraelectric. In this sense, quantum paraelectrics are generally considered incipient ferroelectrics. Therefore, only by small perturbation of external conditions such as replacement of atom, introduction of impurity, application of external field, etc., the system realizes transition to dipole glass state or sometimes to ferroelectric phase at a finite temperature.[6,7]

In $KTaO_3$, the introduction of Li impurity at the K site by a few mol percent (expressed hereafter as KTL or KTL:x%Li in the case where the concentration is significantly important) induces dipole glass state as a result of off-center nature of Li in the lattice.[8] A number of studies have been directed to elucidate the structural property of the system, in particular, whether the long-range ferroelectric phase appears,[9–13] or the polar state induced by Li is localized to remain in the dipole glass state.[14–21] Now the problem seems to be settled: When the Li concentration x exceeds 5 mol %, the para and ferroelectric phase boundary is well defined. In the region of $2<x<3$, the phase boundary becomes obscured, and below the concentration, the dipole glass state is main feature of KTL.[13] As a disordered system conceptually related with spin glass, KTL with $x<3$ is especially important and the peculiar phenomena are expected to be observed. Among them the nonergodic behavior of the order parameter under the external field, is an essential feature of the disordered system. The nonergodicity of the polarization in KTL containing 1.6 and 2.6 % Li was precisely investigated by using the piezoelectric effect,[22] and some other papers also described the related property.[19,21] In this study we use the special nonlinear optical microscope (SHG microscope) which provides two-dimensional (2D) images of optical second-harmonic (SH) waves generated in specimens,[23,24] expecting a new feature of the problem, as SHG is quite sensitive to the appearance and change in the polarization, and the 2D images provide us the polarization distribution inside a specimen, which would be important in the history-dependent experiments. We chose KTL with the critical concentration (2.8%) of Li, and observed the history dependence of the polar state developed under the electric field. SHG measurements of KTL with different concentration of Li have been performed so far. These experiments measured the temperature dependence of SH intensity with and without electric field, for the purpose of determining the spatial correlation length from the k dependence of the scattered SH waves,[25] or from the SHG coherence length.[21] The relaxation time and the activation energy were determined by the kinetic behavior of SH intensity after switching-off the electric field.[21,26] The average symmetry of KTL under the electric field is also discussed[21] based on the result of polarization dependence of the fundamental wave.

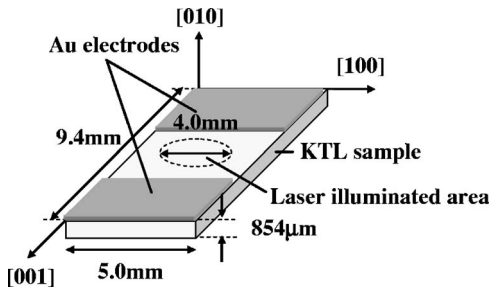

FIG. 1. The orientation and dimension of the specimen used for SHG microscopic observations. A pair of Au electrodes are evaporated on the top surface of KTL. The laser illuminated area is located between two electrodes to avoid the photocurrent effect. The direction of electric field is parallel to [001] referred to the cubic axes.

This paper describes results of the history dependence of SH intensity under the electric field, i.e., zero-field cooling (ZFC), zero-field heating (ZFH), field cooling (FC), and field heating (FH) processes. Special care has been paid to erase the memory effect of specimens. The average symmetry of the polar state induced by the external electric field is determined not only from dependence of the anisotropy of fundamental waves as was previously reported but also from that of SH waves. The result is compared with the x-ray powder diffraction measurement performed down to 10 K on ZFH/ZHC process.

II. EXPERIMENTAL

A. SHG microscopic observations

Specimens used in experiments are KTL:2.8%Li, which were grown by the self-flux method with a slow-cooling technique of Ta_2O_5, Li_2CO_3 and an excess of K_2CO_3 as a flux.[27] Li concentration x was determined by the empirical relation between x and the freezing temperature T_F: $T_F(\mathrm{K}) = 535(x/100)^{0.66}$.[19] T_F was determined from the disappearance temperature of SHG intensity in ZFH after FC process as described later. The homogeneity of Li concentration inside specimens was checked by the distribution of T_F in different illuminated places of the specimen, which is discussed later.

Specimen used in the SHG microscopic observation is a (100) plate (hereafter the axes are referred to the cubic axes), with edges parallel to the {100}, the area 9.4×5.0 mm^2 and the thickness 0.854 mm. Both surfaces are optically finished and two narrow rectangular electrodes apart by 3 mm are put on the top surface by Au evaporation. The orientation and dimension of the specimen are illustrated in Fig. 1. A special care was paid for adjusting the illuminated place of the laser beam so as to be between two electrodes and avoid an occurrence of photocurrent, as KTL exhibits marked photocurrent effect in the low-temperature region.[28–34]

The optical system of SHG microscope is illustrated in Fig. 2. Pulsed waves from Q switched Nd^{3+}:YAG (yttrium aluminum garnet) laser with wavelength of 1064 nm, repetition frequency of 20 Hz, fluence of 15 mW/pulse, pass through a half-wave plate and illuminate a specimen, and SH

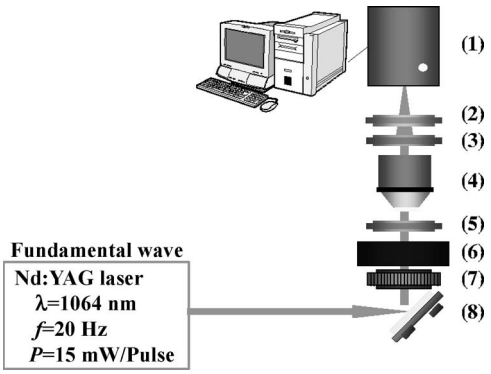

FIG. 2. Optical system of the SHG microscope. (1) CCD camera with image intensifier, (2) 532-nm-pass filter, (3) and (5) infrared absorption filter, (4) objective lens, (6) He cryostat, (7) half wave plate, (8) reflective mirror.

waves with wavelength of 532 nm generated in a specimen are collected by an objective followed by an infrared absorption filter, a multilayer interference filter for 532 nm and an analyzer. Two-dimensional (2D) distribution of SH intensity inside a specimen is obtained by a charge coupled device (CCD) camera with image-intensifier, which is connected to a computer.

The specimen is put in a liquid He cryostat for microscopy (CF2101, Oxford instruments) and the temperature of the specimen is cooled down to 23 K with a speed of 3 K/min, while 1 K/min on heating. Shutter speed (from 5 to 15 s) and gain of CCD camera are selected depending on the SH intensity. Then the temperature change during the exposure time is between 0.1 and 0.75 K.

When the history dependence of SH intensity is observed, the polarizer and the analyzer are fixed along the [001] direction parallel to the applied electric field, while they are rotated along the optic axis when the anisotropy of SH intensity is observed. Comparatively homogeneous areas of 0.075×0.075 mm^2 without a scratch are selected in the two-dimensional SH images and the average intensity are obtained by summing up photon numbers counted by a photodetector array.

B. X-ray-diffraction measurements

A specimen for the x-ray diffraction measurements was prepared by crushing a single crystal of KTL:2.8%Li with small force as possible. The sample powder is mounted on a gilded Cu plate with a small amount of silicon grease. The measurement is performed using a horizontal-type goniometer for powder samples (Rigaku, RINT-TTR3C) equipped with a He cryostat (Rigaku 4 K1) on heating from 10 K with heating speed of 0.5 K/min. Rotating Cu anode ($\lambda_{K\alpha}$=1.5418 Å) is used under the condition of 50 kV and 300 mA. The 400 reflection with $2\theta = 100° - 103°$ is used to determine the lattice constants using a bended graphite monochromator, a divergence slit of 1/2 degree and a receiving slit of 0.15 mm.

III. EXPERIMENTAL RESULTS

A. Observation of the history dependence of SH intensity

The specimen is cooled down to 24 K, then the SH image is observed on heating the specimen up to 100 K. No marked

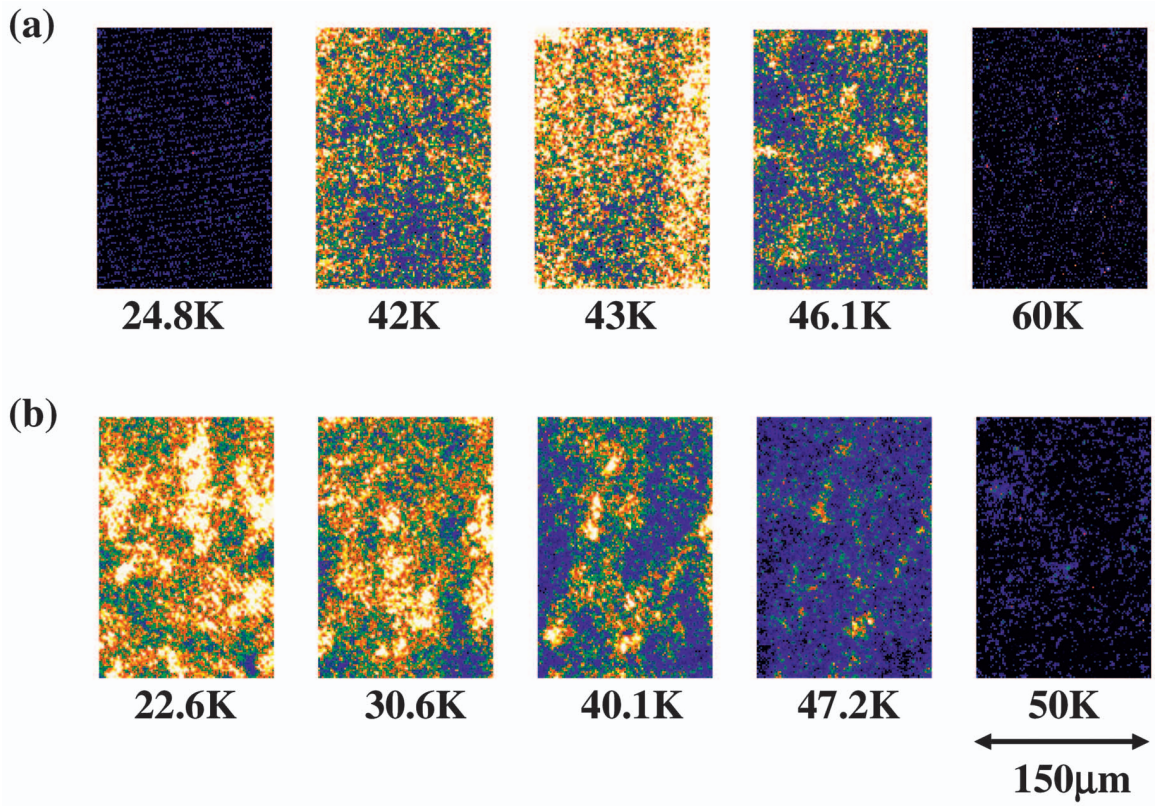

FIG. 3. (Color) SHG images of KTL:2.8%Li. (a) indicates those observed in the FH after ZFC process, (b) in the FH after FC. Brighter parts produce stronger SH waves. In (a), SHG appears only in a limited temperature range below the freezing temperature T_F of 50 K, while in (b), SHG is observed in whole temperature range below T_F.

SH intensity is observed in this process (ZFH/ZFC). Then the specimen is cooled down again down to 24.8 K. The electric field E is applied at the temperature and the specimen is heated up to 60 K under the same field strength. In this process (FH/ZFC), weak SH intensity observed at low temperature starts to increase abruptly at certain temperature T_1, shows a peak and decreases and finally vanishes at a temperature T_2, as shown in Fig. 3(a). T_1 and T_2 depend on the field strength in Fig. 4: The stronger is the field, the lower T_1, the higher T_2, and the stronger the SH intensity. It should be also noted that the SHG intensity is not homogeneously distributed in the sample as shown in SH images (Fig. 3),

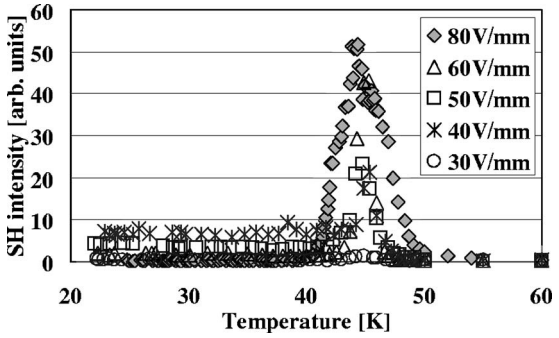

FIG. 4. Temperature dependences of SH intensities of KTL:2.8%Li measured in the FH after ZFC process under different field strengths. In each process, the specimen was kept in room temperature for 12 hours before starting the measurement.

where right spots and dark regions coexist. As the average diameter of bright spots is 1 μm, these are not nanopolar clusters themselves, but the accumulated clusters or the scattered SHG by polar nanoclusters. The dark regions correspond to regions where macroscopic polarization does not develop. Although we cannot perfectly eliminate the possibility that SH intensity vanishes as a result of random distribution of the phase of SH waves produced by polar regions, the possibility would be small as the measurement is performed under the electric field. However, near T_F, the difference of the Li concentration changes the characteristic temperatures, and some parts remains bright but other parts dark. In fact, we observed the T_F differs from place to place in the sample, by 4.0 K. This enables us to estimate the distribution of the Li concentration to be 0.33% in the sample. It is emphasized that the SHG microscopic observations enable us to provide information on the inhomogeneity of materials, while usual SHG measurements cannot do it. In the experiment, we find that the specimen memorizes the previous experience of the field. To erase the memory effect, the specimen is kept at room temperature during 12 h for each run.

We also observed the SH images in FH after FC process. The electric field of 80 V/mm is applied to the specimen at room temperature, the specimen is cooled down to 23 K, then heated up with same field strength. The strong SH intensity is observed at low temperature and gradually decreases with the increase of temperature, and vanishes at 50 K, as shown in Fig. 3(b). In this process, a hump is observed near 45 K, which coincides with the maximum tem-

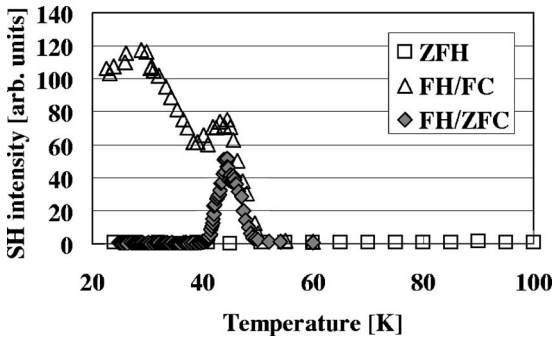

FIG. 5. Temperature dependences of SH intensity of KTL:2.8%Li in ZFC, FH after ZFC and FH after FC processes. The field strength of FC and FH processes is 80 V/mm.

perature in FH/ZFC process. The reason of the appearance of the hump is not clear at present. It could be attributed to the insufficient field strength, which is limited by the strong photoinduced current in KTL, or it would be due to the incomplete erasing of the memory effect. The ZFH after FC process also takes almost same path. The vanishing temperature coincides with that observed in the FH/ZFC with same field strength. Then the temperature (=50 K) can be defined as the freezing temperature T_F of KTL:2.8%Li. Temperature dependences of SH intensity of different paths are summarized in Fig. 5.

B. Anisotropy of SH intensity at low temperature

In order to determine the average symmetry of the field-induced polar state of KTL:2.8%Li, polarization dependences of SH intensity were measured at 23 K after FC process. The procedure of determining the SH intensity is same as in the measurement of the history dependence.

Figure 6(a) shows the SHG intensity as a function of the rotation angle of the polarizer measured with the analyzer fixed parallel to the direction of the electric field ($\parallel$[001]) (case I). A sinusoidal curve of the periodicity of 180° is observed: The maximum is obtained when the polarization direction of the fundamental wave is parallel to the electric field. Similar measurement is made with the analyzer fixed perpendicular to the field direction (case II). A sinusoidal curve of the periodicity of 90° is obtained as shown in Fig. 6(b). Minima are obtained when the polarization direction of the fundamental wave is parallel and perpendicular to the field direction. Then the SH intensities are measured as a function of the polarization direction of the SH wave with the polarizer fixed parallel (case III) and perpendicular to the field direction (case IV), and results are shown in Figs. 6(c) and 6(d), respectively. These results are best fitted with theoretical curves assuming the point group of tetragonal 4 mm as discussed in Sec. IV.

C. Temperature dependence of lattice constants

Powder diffraction profile of (400) reflection spectrum was measured from 10 K with a step of 10 K up to 100 K in ZFH/ZFC process. Examples of the result are indicated in Fig. 7. At low temperature, a split of the profile is observed

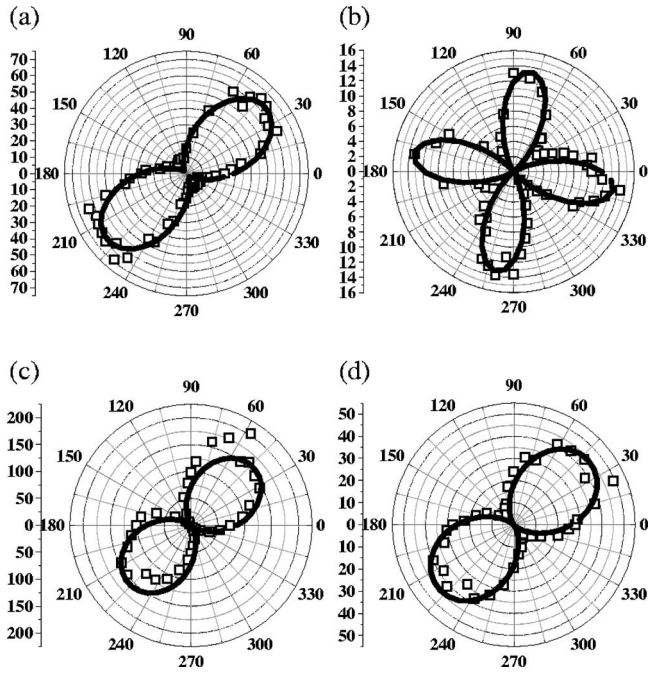

FIG. 6. Polarization dependences of SH intensity of KTL:2.8%. (a) indicates the case I of rotating the polarizer with the analyzer fixed parallel to the electric field $E(\parallel[001])$, (b) the case II of rotating the polarizer with the analyzer fixed perpendicular to E, (c) the case III of rotating the analyzer with polarizer fixed parallel to E, and (d) the case IV of rotating the analyzer with polarizer fixed perpendicular to E. Solid lines indicate fitted curved calculated using Eqs. (1)–(4).

as shown in Figs. 7(a) and 7(b). On the other hand, above T_F, a split disappears and only a well defined peak is observed [Fig. 7(c)]. Lattice constants determined from the analysis are plotted as a function of temperature in Fig. 8. Results of KTO, KTL:1.6%Li, and 5%Li determined by Andrews[13] are

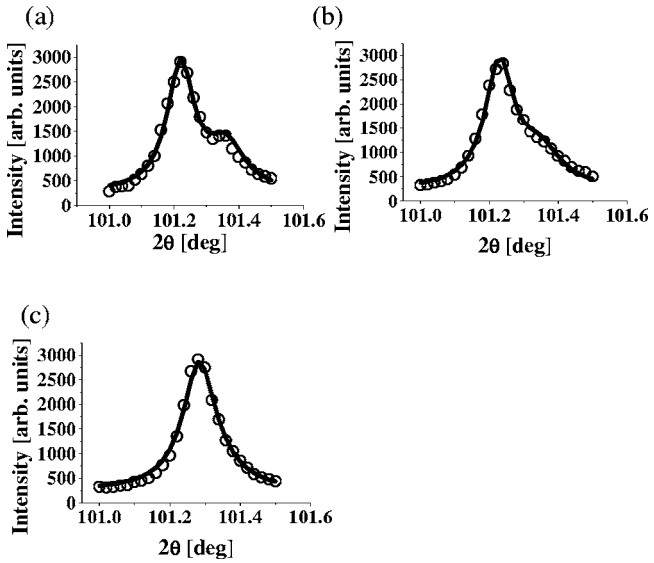

FIG. 7. X-ray powder diffraction profiles of KTL:2.8%. (a) indicates the profile at $T=10$ K, (b) at $T=30$ K, and (c) $T=70$ K, where the Lorentz function is used for the analysis.

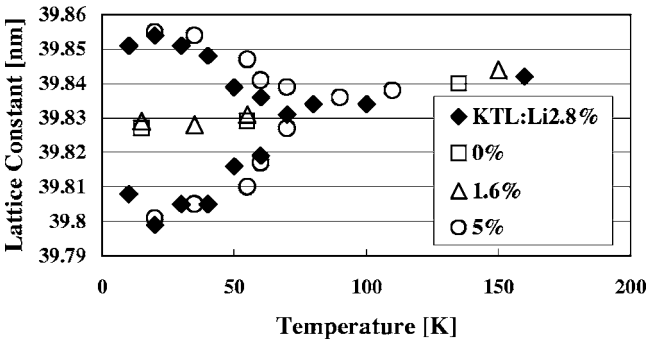

FIG. 8. Temperature dependences of lattice constants of KTL:2.8%. Results of $x=0$, 1.6, and 5 determined by Andrews (Ref. 13) are also plotted for comparison.

also shown for comparison. Our data are located just between those of KTL:1.6%Li and KTL:5%Li. So it is naturally concluded that the macroscopic symmetry of KTL:2.8%Li is tetragonal.

IV. DISCUSSIONS

A. A picture of the polar state of KTL:2.8%Li

Figure 5 obtained in this experiments is quite similar to that in Fig. 4 measured by the piezoelectric effect,[22] however, a difference is observed in the deviation temperature between FH/FC and FH/ZFC. The reason would come from the cooling/heating speed (v). In the present experiment, v is 1 to 3 K/min, while 0.18 K/min in Ref. 22. We managed the experiments with v around the above value, but not with smaller speed mainly due to the temperature-control limit of the optical cryostat. The result confirms a strong evidence for the fact that KTL below the critical concentration is disordered polar state, and no long-range order develops. The dipolar glass state or polar nanoclusters freezes gradually with deceasing temperature below T_F. The application of the external electric field aligns the direction of dipoles produced by off-center Li approximately parallel to the field direction, but it is localized only around Li impurities. At sufficiently low temperature, the freezing of the dipole is so strong that the application of the electric field cannot align the dipole at all. However when the electric field is applied above T_F, a number of dipoles are oriented to the field direction, and the FC process keeps the state down to low temperature. Under strong field, induced dipoles interact each other and ferroelectriclike state is realized. This is a qualitative explanation of the present experiment. It should be stressed that the history dependence shown in Fig. 5 is quite similar to that observed in relaxor $Pb(Mg_{1/3}Nb_{2/3})_3$.[35] As for isothermal relaxation of the polarization, an important discussion has been done on the aging effect of domain size.[36] SHG microscopic observation can prove directly the model, provided that the domain size be comparable or larger than the wavelength, which is the next issue of the investigation.

The present experimental result indicates that the model of polar nanocluster formation in cubic matrix is more relevant in KTL with the critical concentration. The present study did not determine nanocluster size or correlation length of dipole glass. However, several studies have already tackled the problem and obtained a consistent result of the size around 20 nm.[25]

B. Average symmetry of the polar state induced by electric field

To explain the results of Fig. 6, we first assume the point group tetragonal 4 mm with the polar axis parallel to the cubic [001]. Nonzero SHG tensor components d_{ij} (the Voigt notation is adopted here: $i=1-3$, $j=1-6$) are described as follows:

$$\begin{pmatrix} \cdot & \cdot & \cdot & \cdot & d_{15} & \cdot \\ \cdot & \cdot & \cdot & d_{15} & \cdot & \cdot \\ d_{15} & d_{15} & d_{33} & \cdot & \cdot & \cdot \end{pmatrix}.$$

Here Kleinman's law on a transparent nonlinear optical crystal is taken into account. There exist two independent components d_{15} and d_{33}.

SHG intensities I_1, I_2, I_3, and I_4 corresponding to cases I, II, III, and IV are expressed as follows:

$$I_1 = I_{10}^2[\sin^2(\theta-\theta_{10}) + p_1\cos^2(\theta-\theta_{10})]^2, \quad (1)$$

$$I_2 = I_{20}^2[p_2\cos(\theta-\theta_{20})\sin(\theta-\theta_{20})]^2, \quad (2)$$

$$I_3 = I_{30}^2[p_3\cos(\theta-\theta_{30})]^2, \quad (3)$$

$$I_4 = I_{40}^2[p_4\cos(\theta-\theta_{40})]^2. \quad (4)$$

Here $I_{i0}(i=1-4)$ means the intensity of fundamental laser wave, θ_{i0} the direction of the electric field ($\|[001]$), and p_i is expressed using SHG tensor components d_{15} and d_{33} as

$$p_1 = d_{33}/d_{32} = d_{33}/d_{15}, \quad p_2 = 2d_{15},$$

$$p_3 = d_{33}, \quad p_4 = d_{32} = d_{15}. \quad (5)$$

Values determined by fitting experimental results in Fig. 6 are

$$p_1 = 2.82, \quad p_2 = 1.87, \quad p_3 = 2.63, \quad p_4 = 0.92. \quad (6)$$

From these values, the following constant (in arbitrary unit) are consistently obtained:

$$d_{33}/d_{15} = 2.86 \pm 0.18. \quad (7)$$

These values are almost same as the previous reports as shown in Table I.

We assumed that the point group is tetragonal 4*mm*, but our results can be also explained by tetragonal 4, or lower symmetry point group, e.g., orthorhombic *mm*2. However the result of x-ray diffraction experiments shows that the most plausible crystal system is tetragonal. Then the present experiment concludes that the average symmetry of field-induced phase of KTL with Li critical concentration is 4*mm* or 4.

V. CONCLUSIONS

Under the SHG microscope, we observed marked history dependence of the polar phase induced by the electric field in

TABLE I. Experimentally determined SHG tensor component ratio d_{33}/d_{15} of KTL:x%Li.

d_{33}/d_{15}	Li concentration x%	E (V/mm)	Reference
2.86±0.18	2.8	80	Present work
2.51±0.12	0	200	21
2.51±0.12	3.6	0, 80	21
2.45±0.2	1.6, 2.6, 3.4, 6	0	25
2.70±4%	0	2050	37
3.03±4%	0	1530	37

KTL with critical concentration of Li (2.8 mol %). ZFH/ZFC, FH/ZFC, FH/FC, or ZFH/FC processes follow different paths. The result indicates that the ground state of KTL with the critical concentration of Li is intrinsically inhomogeneous where the polar state is localized and the long-range ferroelectric state is not developed. Two models would be plausible: one is polar nanocluster model similar to relaxors, and the other is a dipole glass model. The formation of polar nanoclusters has already reported in pure KTO by using Raman scattering measurements.[38]

The history dependence of the order parameter similar to prototype relaxor PMN seems to support the polar nanocluster model. The marked photocurrent observed in low-temperature region is also consistent with the model, by considering the percolative nature of nanoclusters: If the nanocluster has semiconductive nature, they are connected under the field to generate conductive nets on illumination. For understanding the phenomenon more quantitatively, further experiments are necessary, especially that for disclosing semiconductive nature of the polar nanocluster, e.g., by using scanning prove microscopes. The x-ray diffraction experiments using a single crystal is also waited for.

ACKNOWLEDGMENTS

The work is supported by the grants-in-aid of scientific research (A) of MEXT, the special research program of Waseda University and the 21st century COE program "Physics of systems with self-organization composed of multielements" of MEXT, Japan. We are grateful to Professor Y. Yamada, Professor Y. Tsunoda, Professor K. Kohn, Waseda University, Dr. J. M. Kiat, Ecole Centrale Paris, for valuable discussions, and Mr. Komaki for his help to x-ray measurements, and Mr. Kinoshita for growing single crystals.

*Electronic address: hiroko-9bq@ruri.waseda.jp

[1] S. H. Wemple, Phys. Rev. **137**, A1575 (1964).
[2] C. H. Perry and T. F. McNelly, Phys. Rev. **154**, 456 (1965).
[3] G. A. Samara and B. Morosin, Phys. Rev. B **8**, 1256 (1973).
[4] B. Salce, J. L. Gravil, and L. A. Boatner, J. Phys.: Condens. Matter **6**, 4077 (1994).
[5] J. H. Barrett, Phys. Rev. **86**, 118 (1952).
[6] E. K. H. Salje, B. Wruck, and H. Thomas, Z. Phys. B: Condens. Matter **82**, 399 (1991).
[7] S. A. Hayward and E. K. H. Salje, J. Phys.: Condens. Matter **10**, 1421 (1998).
[8] Y. Yacoby and S. Yust, Solid State Commun. **15**, 715 (1974).
[9] B. E. Vugmeister and M. Glinchuk, Sov. Phys. JETP **52**, 482 (1980).
[10] R. L. Prater, L. L. Chase, and L. A. Boatner, Phys. Rev. B **23**, 5904 (1981).
[11] E. Courtens, J. Phys. C **14**, L37 (1981).
[12] L. L. Chase, E. Lee, R. L. Prater, and L. A. Boatner, Phys. Rev. B **26**, 2759 (1982).
[13] S. R. Andrews, J. Phys. C **18**, 1357 (1985).
[14] U. T. Höchli, H. E. Weibel, and L. A. Boatner, Phys. Rev. Lett. **41**, 1410 (1978).
[15] U. T. Höchli, H. E. Weibel, and L. A. Boatner, J. Phys. C **12**, L563 (1979).
[16] F. Borsa, U. T. Höchli, J. J. van der Klink, and D. Rytz, Phys. Rev. Lett. **45**, 1884 (1980).
[17] I. N. Geifman, A. A. Sytikov, V. I. Kolomytsev, and K. Krulikovskil, Sov. Phys. JETP **53**, 1212 (1981).
[18] U. T. Höchli, Phys. Rev. Lett. **48**, 1494 (1982).
[19] J. J. van der Klink, D. Rytz, F. Borsa, and U. T. Höchli, Phys. Rev. B **27**, 89 (1983).
[20] J. J. van der Klink and S. N. Khanna, Phys. Rev. B **29**, 2415 (1984).
[21] P. Voigt and S. Kapphan, J. Phys. Chem. Solids **55**, 853 (1994).
[22] U. T. Höchli, P. Kofel, and M. Maglione, Phys. Rev. B **32**, 4546 (1985).
[23] Y. Uesu, S. Kurimura, and Y. Yamamoto, Appl. Phys. Lett. **66**, 2165 (1995).
[24] Y. Uesu, R. Nakai, J. M. Kiat, C. Malibert, M. Itoh, and T. Kyomen, J. Phys. Soc. Jpn. **73**, 1139 (2004).
[25] G. A. Azzini, G. P. Banfi, E. Giulotto, and U. T. Höchli, Phys. Rev. B **43**, 7473 (1991).
[26] P. Voigt, S. Kapphan, L. Oliveira, and Maximo Siu Li, Radiat. Eff. Defects Solids **134**, 229 (1995).
[27] J. J. van der Klink, J. Cryst. Growth **56**, 673 (1982).
[28] K. Ohi and S. Iesaka, J. Phys. Soc. Jpn. **40**, 1371 (1976).
[29] E. Yamaichi, Y. Akishige, and K. Ohi, J. Appl. Phys. **23**, 867 (1984).
[30] E. Yamaichi and K. Ohi, J. Appl. Phys. **28**, 1385 (1989).
[31] P. Galinetto, E. Giulotto, P. Sangalli, P. Camagni, and G. Samoggia, J. Phys.: Condens. Matter **11**, 9045 (1991).
[32] R. S. Klein, G. E. Kugel, M. D. Glinchuk, R. O. Kuzian, and I. V. Kondakova, Phys. Rev. B **50**, 9721 (1994).
[33] V. V. Laguta, M. D. Glinchuk, I. P. Bykov, J. Rosa, L. Jastrabik, R. S. Klein, and G. E. Kugel, Phys. Rev. B **52**, 7102 (1995).
[34] P. Sangalli, E. Giulotto, L. Rollandi, P. Calvi, P. Camagni, and G. Samoggia, Phys. Rev. B **57**, 6231 (1998).
[35] K. Fujishiro, T. Iwase, Y. Uesu, Y. Yamada, B. D. Khil, J. M. Kiat, S. Mori, and N. Yamamoto, J. Phys. Soc. Jpn. **69**, 2331 (2000).
[36] F. Alberici-Kious, J. P. Bouchaud, L. F. Cugliandolo, P. Doussineau, and A. Levelut, Phys. Rev. Lett. **81**, 4987 (1998).
[37] Y. Fujii and T. Sakudo, Phys. Rev. B **13**, 1161 (1976).
[38] H. Uwe, K. B. Lyons, H. L. Carter, and P. A. Fleury, Phys. Rev. B **33**, 6436 (1986).

Spectroscopic Observation of Bipolaronic Point Defects in $Ba_{1-x}K_xBiO_3$

Taichiro Nishio,* Javed Ahmad,† and Hiromoto Uwe

Institute of Materials Science, University of Tsukuba, Tennoudai, Tsukuba, Ibaraki, 305-8573, Japan

(Received 22 April 2005; published 18 October 2005)

An infrared-absorption band centered at 0.85 eV, which is below the big optical absorption at the charge-density-wave (CDW) gap energy of 1.85 eV, has been observed for semiconducting single crystalline $Ba_{1-x}K_xBiO_3$. With substituting K for Ba, the spectral weight of the new band increases with x, while that of the CDW-gap excitation decreases. Since the impurity state with the K substitution is known to be nonmagnetic at low temperatures, the Bi^{3+} state with $6s^2$ electrons surrounded by the six Bi^{5+} ions forms a small bipolaron by losing a pair of electrons in the Rice-Sneddon model. The new band is assigned to a transition from the lower-Peierls band to a state of the bipolaronic point defect.

DOI: 10.1103/PhysRevLett.95.176403 PACS numbers: 71.45.Lr, 71.30.+h, 71.38.Mx

For a three-dimensional Peierls semiconductor, $BaBiO_3$ (BBO), a big optical response, has been found at 1.85 eV, which corresponds to the Peierls gap formed by the presence of the short-range order of Bi charge disproportionation [1]. Band-structure calculations [2,3] indicate that BBO, taking a cubic lattice symmetry, would potentially be a high T_c superconductor with high density of states at the Fermi energy and presumable strong electron-phonon interaction, as the band of the Bi $6s$–O $2p$ antibonding state is half filled. The energy gap in the real system possessing monoclinic lattice symmetry arises from the breathing-mode distortion of oxygen octahedra and also the tilting one accompanied by a slight charge disproportionation of Bi atoms. Theoretical calculation [4] by using an extended Peierls-Hubbard model exhibits that direct-exciton excitations on the W-L lines on the boundary surface of the Brillouin zone reproduce the big optical response at 1.85 eV.

When holes are doped, the system should immediately undergo the semiconductor-metal (SM) transition, but a wide range of the semiconductive region is found for $BaPb_xBi_{1-x}O_3$ (BPBO) or $Ba_{1-x}K_xBiO_3$ (BKBO). For BPBO, which is semiconductive for $x < 0.65$, the electron-empty Pb^{4+} band is centered in the upper-Peierls band [1,5]. Because of the increased bandwidth with the considerable Pb doping, the bottom of the Pb band touches the lower-Peierls Bi^{3+} band, thereby inducing the SM transition of the overlapping-band type. Rice and Sneddon [6] have made a model in which Bi $6s$ electrons couple with the breathing-mode distortion of oxygen octahedra to form Bi^{3+} and Bi^{5+} ions. Using a magnetic analog, they have inferred that dilution by the substitution of Pb for Bi causes the SM transition for BPBO.

For BKBO, however, there is no definite interpretation of the wide semiconducting region for $x < 0.3$, although the reflection spectra have been found to exhibit behavior similar to the one in the case of BPBO [7–9]. Recently, using the Rice-Sneddon model in slightly hole-doped BBO, Bischofs, Kostur, and Allen [10] have estimated energy of small polarons or bipolarons, which are self-organized point defects and trap carriers in bound states inside the Peierls gap. They have predicted the bipolaronic point defect which is the state of missing pair of electrons on the nominal Bi^{3+} sublattice. Formation of the small bipolaron may be the mechanism of the insulating state persisting over such a wide range in BKBO.

Here we note that, in optical absorption experiments for BBO, a small indirect energy gap has been found to correspond to the activation energy of the resistivity [11]. Narrowing of the indirect gap has been observed with increase of the substitution in BPBO [12] and also in BKBO [13].

In this Letter, we find a mid-infrared-absorption band centered at 0.85 eV, the spectral weight of which increases with x, while that of the direct transition between the Peierls gap decreases. These indicate that the K-doping destroys locally electron pairs to form the bipolaronic defect states in the charge-density wave (CDW). The result reported here supersedes previous interpretations in optical studies for the semiconducting region of BKBO [7–9,14], in which the new band at 0.85 eV has not been perceived.

For BBO, a single crystal was prepared by slow cooling a stoichiometric mixture of BaO_2 and Bi_2O_3 that was melted in an Al_2O_3 crucible at 1333 K. For BKBO, single crystals were synthesized by an electrochemical method [15]. The K concentrations x of these single crystals were determined by an electron-probe microanalysis (EPMA). A calibration curve between x and the pseudocubic lattice parameter, which is given in Ref. [16], differs from the one for the ceramic samples [17]. All the samples were cut into a form of a flat plate of dimensions $5 \times 4 \times 2$ mm^3 with a large (100) surface that was polished by using Al_2O_3 powder of 0.05 μm in size for the optical measurements. The reflectivity spectra in a frequency range 0.005–0.7 eV were measured on the large surface at $\sim 11°$ incidence by using a Fourier transform spectrometer and those in a frequency range 0.7–4 eV were obtained by a grating spectrometer. All the measurements were carried out at room temperature. The absolute value of the reflectivity

was determined as compared with that of an evaporated Au or Al film, which was measured with the same optical alignment. The dielectric function was obtained by a Kramers-Kronig (KK) transformation of the reflectivity. The experimental data were extrapolated by a curve with the frequency dependence of ω^{-4} from 4 to 17 eV, which was effective for the compensation in the high-frequency ranges.

In Fig. 1 we display the imaginary part of the dielectric function ϵ_2 from the KK analysis. For $x = 0.13$, and 0.16, we clearly find an additional new absorption band B below a primary peak A. The new peak is more conspicuous in the ϵ_2 spectrum than in the conductivity one. The electronic part of the spectrum can be discussed phenomenologically in terms of a Lorentz-oscillator model in which the dielectric function is given by

$$\epsilon(\omega) = \epsilon_{uv} + \sum_j \frac{\omega_j^2 S_j}{\omega_j^2 - \omega^2 - i\omega\gamma_j}, \quad (1)$$

where ω_j, S_j, and γ_j are the frequency, strength, and damping factor of the jth Lorentz optical excitation, respectively, and $\epsilon_{\rm uv}$ is the high-frequency ultraviolet dielectric constant.

In fitting ϵ_2 for $x = 0.13$ and 0.16, we find a sharp feature centered at 1.71 eV, and 1.5 eV (peak A) and another one at 0.85 eV and 0.85 eV (peak B), respectively. For the spectrum of $x = 0.05$, the new band B, also located at 0.85 eV, is weak and difficult to distinguish from the intense peak A at 1.8 eV. In Fig. 2 we show the compositional changes of ω_1 and ω_2 with previous results for single crystals [8,9] or ceramic samples [7] where the peaks A and B were not well resolved. Here, the x values for the single crystals are recalculated by using the calibration curve of the x versus the lattice parameters [16], and the frequencies $\omega_{\rm MAX}$ for the optical conductivity spectra are plotted. Since synthesis of ceramic samples in a semiconductive region is known difficult [18], the frequency in the metallic region is plotted. The position of the peak A is found to decrease with x but remain finite in the beginning of the metallic region, which indicates the pseudogap as in the case of BPBO [1]. The peak A width does

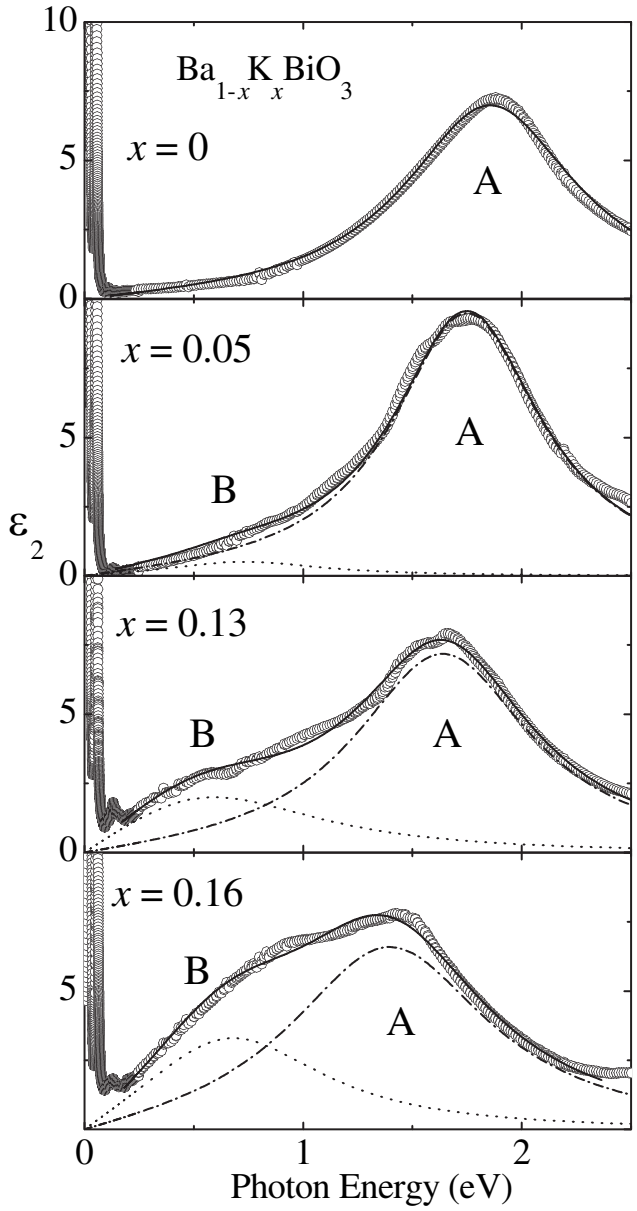

FIG. 1. Imaginary part of dielectric function for semiconductive BKBO. The spectra are decomposed into two Lorentzians of the peak A and B by fitting. The peak B corresponds to an excitation from the lower-Peierls band to the bipolaron- defect state, which increases the intensity with doping. The peak A shifts the position to the lower energy with x.

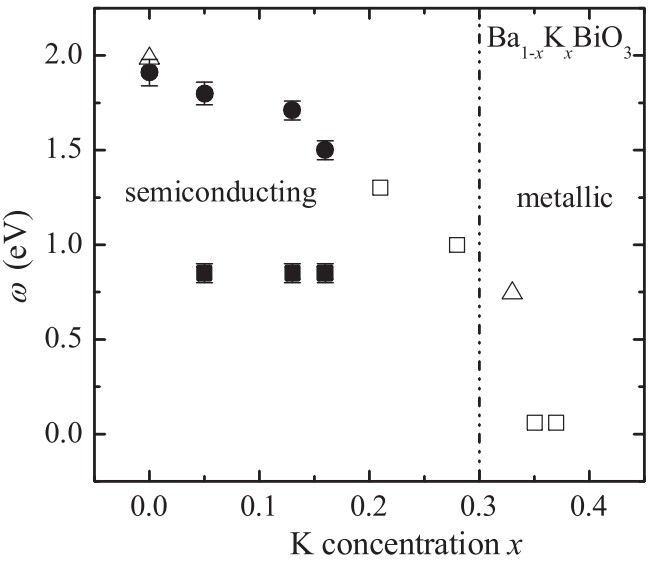

FIG. 2. The peak positions ω_j for the peak A (full circles) and B (full squares). Previous results for single crystals [8,9] (open squares) and ceramic samples [7] (open triangles) are also plotted for the spectra with an apparently single peak.

not change significantly with increasing x (i.e., $\gamma_1 \sim 1.0$ eV). The peak B keeps a nearly constant position of 0.85 eV with doping and has a nearly equal width to the peak A, $\gamma_2 \sim \gamma_1$. With increasing x, we expect that the peak B with a larger width overlaps the peak A with the decreasing position, resulting in a single broad peak in the spectrum.

In Fig. 3, we estimate and plot the effective number of electrons per a Bi atom, N_{eff}, involved in the optical excitations for each absorption band by the following integration,

$$N_{\text{eff}} = \frac{m_0 V_c}{2\pi^2 e^2} \int_0^{\omega_0} \omega' \epsilon_2(\omega') d\omega', \tag{2}$$

where m_0 and V_c are the bare-electron mass and the crystal volume per a Bi atom [19], respectively. For the upper limit of the integral ω_0, the cutoff frequency should be used, since the Lorentzian function is known to have a long tail. We use the frequency giving the minimum of the optical conductivity spectrum in accordance with the definition of Ref. [9]. In Fig. 3, it is found that N_{eff} at $x = 0$ is 0.5 by a factor of $1/2$ smaller than 1 electron per Bi, which should be involved in the excitation across the CDW gap assuming no transition to the higher levels, as Puchkov *et al.* [9] have pointed out as the missing spectral weight.

For the peak B component, we find that the N_{eff} increases with doping and approaches the substantial part of the reported values for the overdamped midinfrared component in the metallic region [9,20]. On the other hand, that of the peak A increases once and decreases with x.

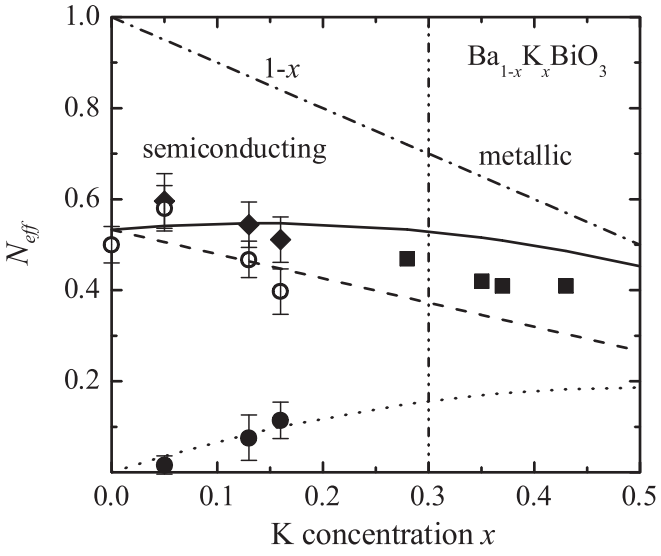

FIG. 3. Spectral weight for the peak A (open circles), B (full circles), the sum (full diamonds), and the previous results (full squares) [8,9]. The broken, dotted, and solid lines are fits to the spectral weights of $a(1-x)/4$, $b(1-x)x/4$, and the sum, respectively, in which the expressions take account of the bipolaron concentration with the doping. The chain line is $N_{\text{eff}} = 1 - x$.

In the Rice-Sneddon model, in which the strong interaction is taken into consideration between electrons and the breathing-mode distortion in BKBO, the doped holes are shown to be self-trapped to result in small polarons or small bipolarons [10,21]. The small bipolaron is predicted more stable than the small polarons and amounts to a point defect. Absence of local-intrinsic-moment behavior in doping systems [22,23] is consistent with the small-bipolaron picture. The predicted energy level of the small bipolaron in the Peierls gap of 2Δ is located at $0.7\Delta = 0.7$ eV above the lower-Peierls band compatible with the experimental observation of 0.85 eV.

The number of the bipolaron states per a Bi atom is $x/2$, and that of the lower band, i.e., Bi^{3+} states, decreases as a function of $(1-x)/2$. Thus, the weight of the transition from the lower band to the small-bipolaron state changes as $bx(1-x)/4$; on the other hand, that from the lower to higher Peierls band should decrease as $a(1-x)/4$. We note that a and b would be constants as long as x is small and the transition matrix elements between the states remain constant with x. In Fig. 3, we plot the fits to the spectral weights for the peaks A and B, where $a = 2.13$ and $b = 2.98$. The total spectral weight of A and B is close to the previous data even in the more concentrated region [9]. Therefore, the optical spectrum below 1.85 eV in the metallic region seems to be comprised of the peaks A, B and the Drude component from the free carriers, in accordance with the experimental observation [20] that the optical conductivity for $x = 0.4$ consists of two contributions; one is a Drude-like component (about 6% of the midinfrared one) and another is an overdamped Lorentz component centered at ~ 0 eV.

Since the electronic wave function compatible with the CDW would be expressed as $\cos\frac{\pi}{2}x \cos\frac{\pi}{2}y \cos\frac{\pi}{2}z$ and the wave function at the bipolaron point defect is the s state at the origin, the optical transition is forbidden [10]. In the realistic band calculation [3] for BBO, the top of the lower band is predicted to be the W-point state, though the optical transition to the bipolaronic point defect would still be forbidden. In BBO, however, LO phonons are found both infrared and Raman active, which indicates that BBO lacks inversion symmetry [24]. Although a compatible local or uniform crystal structure is unknown, the local structure seems different from the mean crystal structure measured by the neutron or x-ray diffraction method, and the observed peak B transition is optically allowed, since the N_{eff} is close to the K content or the doped-hole one. For the peak A, the reason for the first increase of N_{eff} at $x = 0.05$ may possibly be due to the increase of the local distortion around Bi^{5+} ions adjacent to the bipolaron defects which appear with the doping.

According to Bischofs, Kostur, and Allen [10], as a result of the hole doping, the Bi^{5+} bipolaron state occurs at the Bi^{3+} site, and a single bipolaron distortion changes six adjacent Bi^{5+} states to six localized ones for electrons

below the bottom of the unoccupied upper-Peierls band. With increasing doping, these localized states will have width just like the impurity band, since the electronic wave functions become to overlap each other between the localized states. Therefore, the width of the upper-Peierls band increases and the peak position of the spectrum A decreases with the doping. Furthermore, two bipolarons adjacent to a Bi^{5+} upper-Peierls state will appear with doping and make the localized state with further lowering its energy. Since the peak B position keeps constant in the semiconducting region, the system is inferred to undergo the SM transition, when the bottom of the upper-Peierls band crosses the top of the lower-Peierls band on lowering the energy with the interaction between the Bi^{5+} site and the adjacent several bipolaron defects.

For the semiconducting sample near the SM transition, the bipolaron transport is claimed from the optical conductivity spectrum [14], which seems, however, to be assigned as the merged feature of the peak A and B, as has been discussed above for Figs. 2 and 3. Observed peak of the bipolaron is due to the interband transition, not the intraband one. Since the indirect gap was found in the optical absorption spectrum [13], the electrons and holes are thermally excited across the gap, so that small electron polarons and hole ones rather than small bipolarons seem to play important role in the transport phenomena as a result of the strong electron-phonon interaction. The bipolaron which appears with the K substitution for Ba will reside near the K site because of the Coulomb interaction. At high temperatures up to 400 K, a new excitation [25,26] appears below the peak B, and at low temperatures the behavior of the finite optical conductivity was found at the far-infrared region [27], which indicates the small-polaron excitation.

In summary, in the system of BKBO, there are two components in the optical spectra below 1.85 eV; one corresponds to the CDW-gap excitation from the lower to upper-Peierls band, and another to the transition from the lower-Peierls band to the bipolaron local defects in the semiconducting region, and both remain even in the metallic region.

We thank N. Nishida, the Chemical Analysis Center, for the help of EPMA.

*Present address: Kamerlingh Onnes Laboratory, University of Leiden, The Netherlands.

†On leave from Department of Physics, Bahauddin Zakariya University, Multan, Pakistan.

[1] S. Tajima, S. Uchida, A. Masaki, H. Takagi, K. Kitazawa, S. Tanaka, and A. Katsui, Phys. Rev. B **32**, 6302 (1985).

[2] L. F. Mattheiss and D. R. Hamann, Phys. Rev. B **28**, 4227 (1983).

[3] A. I. Liechtenstein, I. I. Mazin, C. O. Rodriguez, O. Jepsen, O. K. Andersen, and M. Methfessel, Phys. Rev. B **44**, R5388 (1991).

[4] S. M. Hasanuzzaman, K. Iwano, and K. Nasu, J. Phys. Soc. Jpn. **68**, 1376 (1999).

[5] H. Namatame, A. Fujimori, H. Takagi, S. Uchida, F. M. F. de Groot, and J. C. Fuggle, Phys. Rev. B **48**, 16 917 (1993).

[6] T. M. Rice and L. Sneddon, Phys. Rev. Lett. **47**, 689 (1981).

[7] S. H. Blanton, R. T. Collins, K. H. Kelleher, L. D. Rotter, Z. Schlesinger, D. G. Hinks, and Y. Zheng, Phys. Rev. B **47**, 996 (1993).

[8] M. A. Karlow, S. L. Cooper, A. L. Kotz, M. V. Klein, P. D. Han, and D. A. Payne, Phys. Rev. B **48**, 6499 (1993).

[9] A. V. Puchkov, T. Timusk, M. A. Karlow, S. L. Cooper, P. D. Han, and D. A. Payne, Phys. Rev. B **54**, 6686 (1996).

[10] I. B. Bischofs, V. N. Kostur, and P. B. Allen, Phys. Rev. B **65**, 115112 (2002).

[11] H. Uwe and K. Tachibana, *Advances in Supercond.* (Springer, New York, 1995), Vol. VII, p. 165.

[12] H. Uwe and Y. Yamamoto, *Proceedings of the 21st International Conference on Low Temperature Physics*, edited by S. Danis, V. Gregor, and K. Záveta (World Scientific, Singapore, 1996), p. 2689.

[13] M. E. Kozlov, X. Ji, H. Minami, and H. Uwe, Phys. Rev. B **56**, 12 211 (1997).

[14] A. V. Puchkov, T. Timusk, M. A. Karlow, S. L. Cooper, P. D. Han, and D. A. Payne, Phys. Rev. B **52**, R9855 (1995).

[15] T. Nishio, H. Minami, and H. Uwe, Physica C (Amsterdam) **357-360**, 376 (2001).

[16] T. Nishio and H. Uwe, J. Phys. Soc. Jpn. **72**, 1274 (2003).

[17] S. Pei, J. D. Jorgensen, B. Dabrowski, D. G. Hinks, D. R. Richards, A. W. Mitchell, J. M. Newsam, S. K. Sinha, D. Vaknin, and A. J. Jacobson, Phys. Rev. B **41**, 4126 (1990).

[18] A. Iyo, H. Uwe, and T. Sakudo, *Advances in Supercond.* (Springer, New York, 1992), Vol. IV, p. 211.

[19] Pseudocubic lattice parameters for estimating V_c are shown in Ref. [16].

[20] A. V. Puchkov, T. Timusk, W. D. Mosley, and R. N. Shelton, Phys. Rev. B **50**, 4144 (1994).

[21] J. Yu, X. Y. Chen, and W. P. Su, Phys. Rev. B **41**, 344 (1990).

[22] B. Batlogg, R. J. Cava, L. W. Rupp, Jr., A. M. Mujsce, J. J. Krajewski, J. P. Remeika, W. F. Peck, Jr., A. S. Cooper, and G. P. Espinosa, Phys. Rev. Lett. **61**, 1670 (1988).

[23] H. Uwe, X. Ji, and H. Minami, *Proceedings of the 21st International Conference on Low Temperature Physics*, edited by S. Danis, V. Gregor, and K. Záveta (World Scientific, Singapore, 1996), p. 2691.

[24] S. Sugai, Phys. Rev. B **35**, 3621 (1987).

[25] J. Ahmad, T. Nishio, and H. Uwe, Physica C (Amsterdam) **388-389**, 455 (2003).

[26] J. Ahmad and H. Uwe, Phys. Rev. B **72**, 125103 (2005).

[27] J. Ahmad and H. Uwe, Physica C (Amsterdam) **412-414**, 288 (2004).

Phase Transition in Bi-layered perovskite and a model of ultra-thin ferroelectric film

Akira ONODERA

Department of Physics, Hokkaido University, Sapporo 060-0810, Japan

Ferroelectricity in Bi-layered pseudo-perovskite $SrBi_2Ta_2O_9$ (SBT) was discovered at 608 K (T_c) by Smolenski *et al* in 1961 [1]. $SrBi_2Ta_2O_9$ has been much attracted as a promising material for ferroelectric nonvolatile semiconductor memory (FeRAMs) [2,3] and optoelectronic integrated devices. The crystal structure of SBT is highly anisotropic and is composed from $SrTa_2O_7$ perovskite-like unit sandwiched by bismuth oxide semiconductor layers. This structural character is just suitable for fabrication of thin films and might be a key material of future ferroelectric-device application. The spontaneous polarization (P_s) is relatively large (5.8 $\mu C/cm^2$ along the *a*-axis at room temperature), while P_s=26 $\mu C/cm^2$ in a representative perovskite ferroelectric $BaTiO_3$ along the tetragonal *c*-axis. The dielectric constant (ε) and the specific heat (C_p) of this crystal show very weak and broad temperature dependence with 100 K temperature width. The peak value of e is only 300 at T_c, which is two orders as small as that of $BaTiO_3$. Although these two perovskite oxides exhibit quite different nature, the dielectric behavior of $BaTiO_3$ thin film is rather similar to those in SBT. Based on this analogy, we will expect that this bulk layered ferroelectric is a good example of ultra-thin ferroelectric model with 2 monolayers of TaO_6 perovskite units, free from any misfit lattice strain with substrate.

We studied thermal and structural behavior of SBT, and found anomalies at 608 K (T_c) and 850 K (T*) in C_p and lattice constants by X-ray diffraction [4-5]. X-ray Rietveld analysis confirmed the tetragonal structure over T* and antiparallel arrangements of TaO_6 octahedra in the high-temperature paraelectric phase above 850 K. The TaO_6 octahedra are distorted along the *c*-axis. In the ferroelectric phase, this crystal favors canted octahedral arrangements below T_c, which result in the net

spontaneous polarization along the *a*-axis. We suggest canted ferroelectricity (weak ferroelectricity) for SBT.

References

[1]. G. A. Smolenskii, V. A. Isupov and A. I. Agranovskaya: Sov. Phys. - Solid State **3,** 51 (1961).

[2]. C. A-Paz de Araujo, J. D. Cuchiaro, L. D. McMillan, M. C. Scott and J. F. Scott: Nature **374,** 627 (1995).

[3]. J. F. Scott: Ferroelectrics Review **1,** 1 (1998).

[4]. A. Onodera, K. Yoshio, C.C. Myint, S. Kojima, H. Yamashita and T. Takama: Jpn. J. Appl. Phys. **38,** 5683 (1999).

[5]. A. Onodera, T. Kubo, K. Yoshio, S. Kojima, H. Yamashita and T. Takama: Jpn. J. Appl. Phys. **39,** 5711 (2000).

Universality of the lead-free piezoelectric solid solution $(Na,K)NbO_3$-$ATiO_3$

Ruiping WANG

Nanoelectronics Research Institute
National Institute of Advanced Industrial Science and Technology

Recently, it is reported that $(Na,K)NbO_3$-based lead-free piezoelectric ceramics with properties that closely match those of lead zirconium titanate (PZT) have been created [1]. This result has established a firm position for the $(Na,K)NbO_3$-based solid solutions as the most prospective lead-free piezoelectric alternatives for PZT. In order to study the mechanism responsible for the doping-enhanced piezoelectricity in $(Na,K)NbO_3$-based solid solutions, the dielectric and the piezoelectric properties of the solid solution $(Na,K)NbO_3$-$ATiO_3$ (A = Ba, Sr, and Ca) have been studied [2-4].

Barium titanate ($BaTiO_3$), strontium titanate ($SrTiO_3$), and calcium titanate ($CaTiO_3$) have the same perovskite structure as $(Na,K)NbO_3$ and a complete solid solution can be formed between them. According to the dielectric constant measurement results, a phase diagram is established for each solid solution (Fig. 1). It is found that, for $(1-x)(Na,K)NbO_3$-$xATiO_3$ (A = Ba, Sr, and Ca) solid solution, piezoelectric properties, dielectric properties and the phase diagrams show following universalities: (1) the cubic-tetragonal (C-T), the tetragonal- orthorhombic (T-O), and the orthorhombic-rhombohedra phase transition temperatures rapidly decrease with increasing x. (2) the dielectric constant peaks become more and more broadened with increasing x. (3) the T-O phase transition temperature (t_{c2}) decreases more sharply than the C-T phase transition temperature (t_{c1}) does. Moreover, t_{c2} is only a function of x and almost independent of A. (4) a T/O morphotropic phase boundary (MPB) is formed at $x \sim 0.05$. (5) the electromechanical coupling coefficients k_p and the piezoelectric constant d_{33} maximize at around $x \sim 0.05$.

According to the above results, we suggest that the mechanism responsible for the enhanced piezoelectric properties in the

(Na,K)NbO_3-based solid solutions is the T/O MPB formation at x ~ 0.05.

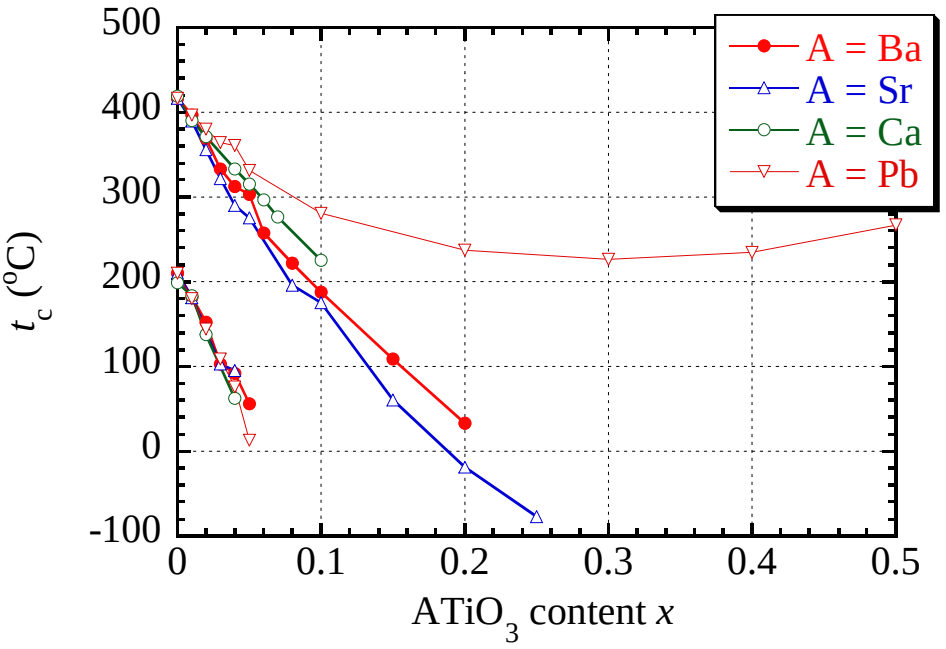

Fig. 1 Phase diagram summarized from the dielectric constant measurements.

References

[1]. Y. Saito, H. Takao, T. Tani, T. Nonoyama, K. Takatori, T. Homma, T. Nagaya, and M. Nakamura: Nature **432,** 84 (2004).

[2]. R. Wang, R.-J. Xie, K. Hanada, K. Matsusaki, H. Bando and M. Itoh: Phys. Stat. Sol. **202,** R57 (2005).

[3]. R. Wang, R-J Xie, T. Sekiya, Y. Shimojo, Y. Akimune, N. Hirosaki, and M. Itoh: Ferroelectrics **286,** 93 (2003).

[4]. R. Wang, R-J Xie, T. Sekiya, Y. Shimojo, Y. Akimune, N. Hirosaki, and M. Itoh: Jpn. J. Appl. Phys. **41,** 7119 (2002).

Ferroelectric domain structures near the MPB of $Pb(Zr_{1-x}Ti_x)O_3$

Toshihiro ASADA[*] and Yasumasa KOYAMA[*,**]

[*]*Kagami Memorial Laboratory of Materials Science and Technology, Waseda University*
[**]*Department of Materials Science and Engineering, Waseda University*

$Pb(Zr_{1-x}Ti_x)O_3$におけるMPB近傍の強誘電分域構造

浅田敏広[*]、小山泰正[*,**]
[*]早稲田大学 各務記念材料技術研究所
[**]早稲田大学 理工学部　物質開発工学科

強誘電体 $Pb(Zr_{1-x}Ti_x)O_3$(PZT)の Ti 置換量 x=0.48 付近には、温度軸に対してほぼ垂直なモルフォトロピック相境界(MPB)と呼ばれる、菱面体晶/正方晶相境界が存在する。最近 Noheda らは、MPB 付近での結晶構造の特徴をシンクロトロン放射光を用いて調べ、顕著な圧電性に関係する強誘電単斜晶相の存在を明らかにしている [1]。そこで本研究では、単斜晶相を含めた MPB 付近に現れる各相の強誘電分域構造の特徴を、透過型電子顕微鏡を用いたその場観察により明らかにした。

実験に供した試料は、固相法により作製した $0.40 \leq x \leq 0.55$ 組成域の PZT 試料である。透過型電子顕微鏡用試料は、これら PZT 試料を Ar イオンミリングすることにより作製した。作製した試料の強誘電分域構造の特徴については、JEM-3010(300kV)透過型電子顕微鏡を用い、室温から 873K の温度範囲において電子回折図形ならびに明･暗視野像を撮影することにより明らかにした。特に本研究では、各強誘電分域での分極ベクトルの向きを決定するため、フリーデル則の破れを生じる二波励起条件のもと、**g** および**-g** の一対の暗視野像を撮影した。

観察の結果、$0.46 \leq x \leq 0.48$ に存在する強誘電単斜晶相において、3 種類の強誘電分域構造の存在が明らかとなった。ここで、その顕著な特徴は、菱面体晶／単斜晶相境界付近の分域構造が 10nm 程度の強誘電ナノ分域からなることである。さらに菱面体晶相での室温からの試料の加熱により、109 ° 分域から成る通常の分域構造が大きさ約 10nm のナノ分域構造へと、分域構造変化することも分

かった。特に、この分域構造変化は、加熱および冷却により、連続的かつ可逆的に生じることも確認された。講演では、これら得られた実験データの詳細について報告する。

References

[1]. Noheda *et al.*: Appl. Phys. Lett. **74,** 2059 (1999).

Order-disorder Nature of New Ferroelectric $BaTi_2O_5$

Anwar HUSHUR[*)], Hirotake SHIGEMATSU[a)], Yukikuni AKISHIGE[a)] and Seiji KOJIMA

Institute of Materials Science, University of Tsukuba, Tsukuba, Ibaraki 305-8573, Japan
[a)]Faculty of Education, Shimane University, Matsue, Shimane 690-8504, Japan

Lead-based ferroelectric materials with perovskite structure, PZT and PMN-PT, exhibit good ferroelectric and piezoelectric properties, and thus are widely used as electromechanical devices. However, lead may affect natural environment. The development of lead-free ferroelectric materials is required from the viewpoint of environmental problems. Very recently, Akishige *et al.* found ferroelectricity in $BaTi_2O_5$ single crystal. The crystal system of the ferroelectric phase is monoclinic with space group C2 and has a spontaneous polarization of 7 μCcm^{-2} along the *b*-axis. However, in our knowledge, minimal information is available regarding the physical properties and dynamics of the ferroelectric phase transition of this material. To clarify the origin of ferroelectricity, an important point is to know whether this transition is primarily of displacive or of order-disorder type. In present work, ferroelectric single crystals of $BaTi_2O_5$ have been studied in detail by Raman and high-resolution micro-Brillouin scattering with focus on the central component of the relaxation mode over a wide temperature range (20 – 600^{o}C). A relaxation mode has been clearly observed in these single crystals for the first time. The temperature dependence of the relaxation time and integrated intensity of the relaxation mode are well reproduced by the extended semiclassical tunneling model. The ferroelectric phase transition shows, at least near the vicinity of T_c, an order-disorder nature. Our results indicating that the spontaneous polarization mainly resulted from the dynamic disorder of the Ti ions in the octahedra along the polar *b*-axis of $BaTi_2O_5$.

Order-disorder nature of ferroelectric $BaTi_2O_5$

Anwar Hushur[a)]
Institute of Materials Science, University of Tsukuba, Tsukuba, Ibaraki 305-8573, Japan

Hirotake Shigematsu and Yukikuni Akishige
Faculty of Education, Shimane University, Matsue, Shimane 690-8504, Japan

Seiji Kojima
Institute of Materials Science, University of Tsukuba, Tsukuba, Ibaraki 305-8573, Japan

(Received 8 September 2004; accepted 18 January 2005; published online 7 March 2005)

Ferroelectric single crystals of $BaTi_2O_5$ have been studied in detail by Raman and high-resolution micro-Brillouin scattering with a focus on the central component of the relaxation mode over a wide temperature range (20–600 °C). A relaxation mode has been clearly observed in these single crystals. The temperature dependences of the relaxation time and integrated intensity of the relaxation mode are well reproduced by the extended semiclassical tunneling model. The ferroelectric phase transition shows, at least near the vicinity of T_c, an order-disorder nature. Our results indicate that the spontaneous polarization mainly resulted from the dynamic disorder of the Ti ions in the octahedra along the polar *b* axis of $BaTi_2O_5$. © *2005 American Institute of Physics*. [DOI: 10.1063/1.1880442]

Lead-based ferroelectric materials with perovskite structure, lead zirconium titanate (PZT) and lead magnesium niobate-lead titanate (PMN-PT), exhibit good ferroelectric and piezoelectric properties, and thus are widely used as electromechanical devices. However, lead may affect the natural environment. The development of lead-free ferroelectric materials is required from the viewpoint of environmental problems. Barium titanate ($BaTiO_3$) is a good candidate for a lead-free ferroelectric material. Usually A- and B-site dopants have been used to modify the electrical properties of $BaTiO_3$. In this way, either or both the Curie temperature T_c and the nature of a phase transition may be modified and sometimes lead to a diffuse phase transition-type behavior.[1] Statton[2] grew single crystals of barium dititanate ($BaTi_2O_5$) together with $BaTi2O_3$, $BaTi_4O_9$, and Ba_2TiO_4 to investigate the binary system of $BaO-TiO_2$ in the 1950s. Harrison[3] and Tillmanns[4] determined that its crystal system is monoclinic with space group C_{2h}. Very recently, Akishige *et al.*[5,6] found ferroelectricity in this single crystal. The crystal system of the ferroelectric phase is monoclinic with space group C2 and has a spontaneous polarization of 7 μC cm^{-2} along the *b* axis. The unit-cell parameters are $a=16.91$ Å, $b=3.94$ Å, $c=9.49$ Å, and $\beta=103.0°$. Dielectric measurements show that the ferroelectric $BaTi_2O_5$ crystal grown in a reducing air shows a diffuse phase transition at around $T_c \sim 430$ °C. The crystal grown in air shows a sharp dielectric anomaly reaching 30 000 at $T_c \sim 479$ °C. Kimura *et al.*[7] shows the displacement of Ti atoms in the one of the Ti sites is mainly responsible for the ferroelectricity. Furthermore, ferroelectricity of this single crystal was confirmed and explained using first-principle calculation.[8] However, except dielectric measurements, minimal information is available regarding the physical properties and dynamics of the ferroelectric phase transition of this material. To clarify the origin of ferroelectricity, an important point is to know whether this transition is primarily of displacive or of order-disorder type.[9]

To understand the phase transition mechanism at T_c and lattice dynamics, it is useful to apply an inelastic light scattering technique. Since, frequency shifts and full width at half maximum (FWHM) of the optical and acoustical modes are very sensitive to phase transitions and also low frequency, relaxation phenomena can be directly observed by this method. Here, we report on the normal modes and central peak of $BaTi_2O_5$ single crystals by the Raman and Brillouin light scattering technique.

Needlelike crystals of $BaTi_2O_5$ were grown by rapidly cooling fine powders of $BaTiO_3$ and TiO_2 as starting materials. The consequent mixing ratio is $BaO:TiO_2=33:67$. Crystal growth was performed in air ambient. Details of the growth conditions have been reported elsewhere.[5,6] Raman scattering is excited using a diode-pumped solid-state laser at a wavelength of 532 nm and a power of about 100 mW. The signal was analyzed by a triple-grating spectrometer of additive dispersion (Jobin Yvon T64000). The spectral resolution was about 2 cm^{-1}. The Brillouin scattering spectra were measured using a (3+3) tandem Fabry–Perot interferometer of high contrast, combined with an optical microscope (OLYMPUS BH-2). A conventional photon-counting system and a multichannel analyzer were used to detect and average the signal. A single-frequency Ar^+-ion laser with a wavelength of 514.5 nm and power of 100 mW was used to excite the sample. In both methods, backward scattering geometry was employed. A cryostat cell (THMS 600) with temperatures varying from −190 °C to 600 °C and with a stability of ±0.1 °C was used for temperature variation.

The temperature dependence of the Raman spectra of a $BaTi_2O_5$ single crystal measured in $a(b,b+c)\bar{a}$ geometry from 8 cm^{-1} to 120 cm^{-1} is shown in Fig. 1. No soft mode was observed. The lowest mode appeared at 80 cm^{-1} at room temperature where indicated by arrows. Although, the mode frequency of this lowest mode does not show clear softening, it shows broadening approaching T_c then disappears. A typical Brillouin spectra with a free spectral range (FSR) of 100 GHz and a scan range of 1.5 FSR on a (100) plane at selected temperatures are shown in Fig. 2. Both methods, in

[a)]Author to whom correspondence should be addressed; electronic mail: anwar@ims.tsukuba.ac.jp

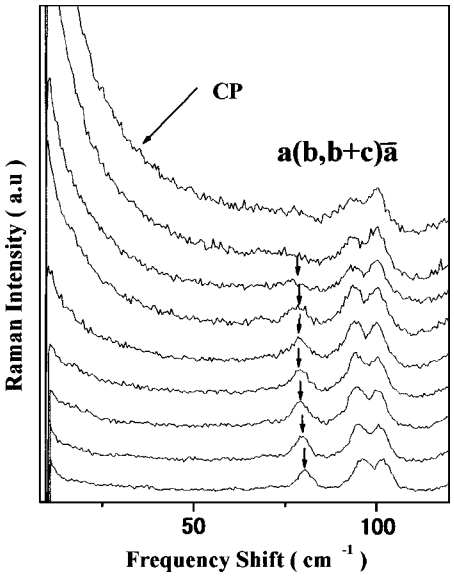

FIG. 1. Low-frequency Raman spectra in $BaTi_2O_5$ obtained between 8 cm^{-1} and 120 cm^{-1} at temperatures 500, 440, 380, 320, 260, 200, 140, 80, and 20 °C, from top to the bottom. The arrows indicate the lowest mode observed at 80 cm^{-1} at room temperature. CP indicates central peak.

addition to the usual phonon features, such as normal modes determined by selection rules, a relaxation mode has been clearly observed in $BaTi_2O_5$ crystals. Upon heating, a central peak appears around 300 °C and shows marked temperature dependence. The intensity of the central peak increases markedly as the temperature approaches T_c from both above and below. The spectral analysis on Brillouin spectra was carried out using the convolution of a Lorentzian spectral function with a Gaussian broadening function. The temperature dependences of elastic stiffness constant c_{66} obtained from frequency shifts and FWHM for the transverse acoustic (TA) mode are shown in the inset of Fig. 3. One anomaly is clearly observed at T_c=470 °C from both c_{66} and FWHM of the TA mode. The transition temperature reported here is in good agreement with those obtained by dielectric measurements for $BaTi_2O_5$ of the same sample.[5] The elastic stiffness constant c_{66} shows a softening upon approaching T_c from below. However, above T_c, it does not show any clear temperature dependence. The interesting part is above T_c, where

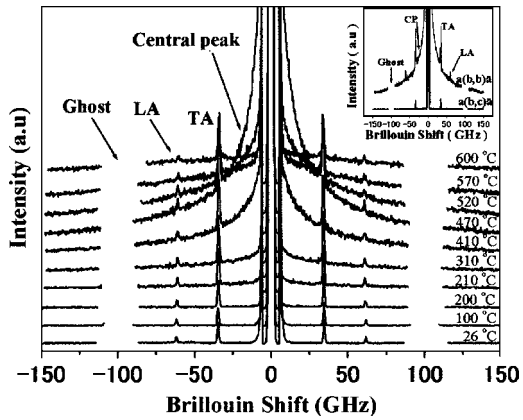

FIG. 2. Brillouin spectra obtained with FSR of 100 GHz and scan range of ±1.5 FSR at temperatures 600, 570, 520, 470, 410, 350, 310, 200, 100, and 26 °C, respectively, from the top to the bottom. LA: longitudinal acoustic mode. TA: transverse acoustic mode. Inset: Polarization dependence of Brillouin spectra of $BaTi_2O_5$ at 410 °C.

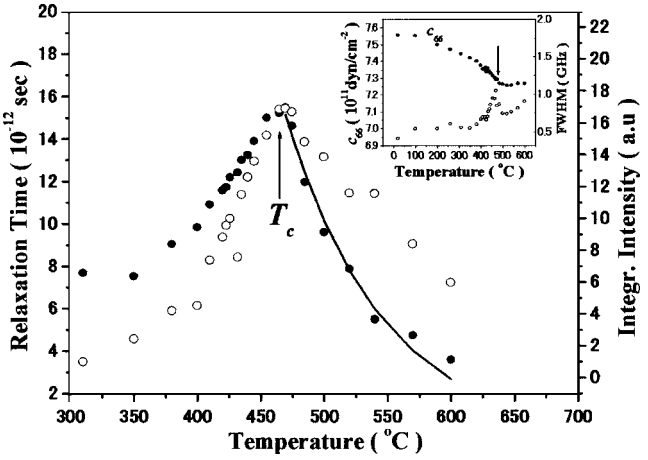

FIG. 3. The temperature dependence of the integrated intensity (open circle) and the relaxation time τ (dark circle) of the relaxation mode of $\mathbf{q}\|a$. Solid line is the fit of the relaxation times using the tunneling model, with $1/\tau_0$ =670 cm^{-1}, ΔV=821 cm^{-1}. Inset: Elastic stiffness constants c_{66} (dark circle) and FWHM (open circles) for the TA mode. The arrow indicates the phase transition temperature T_c.

we can still see the hypersonic damping. This observation correlated with the appearance of a central peak, as shown in Fig. 2. Here, we will focus on the properties of the relaxation mode; The acoustic properties will be published separately.

When the relaxation occurs in the ionic motion, the spectral response $S(\omega)$ is usually well described by the Debye relaxation in the high-temperature approximation.

$$S(\omega) = \chi''(\omega)[n(\omega) + 1] \propto \frac{1}{1 + \omega^2\tau^2}, \tag{1}$$

where $S(\omega)$ is approximated by a Lorentzian centered at zero-frequency shift with a half width at half maximum equal to the inverse of the relaxation time τ.

The obtained intensity of the central peak and the relaxation time are shown in Fig. 3. It can be noted that the anomalies are observed in both intensity and relaxation time at around 470 °C, which is the same temperature as the anomalies of the acoustic anomalies shown in Fig. 2. The relaxation time slows down and the central peak intensity increases markedly when temperature approaches T_c from above and below. However, the rate of slowing down is different above and below T_c. Point symmetry of $BaTi_2O_5$ at room temperature is monoclinic C_2; $a(b,b)\bar{a}$ scattering geometry relates to A(y)-symmetry excitation, which involves ionic motion parallel to the polar axis, and $a(b,c)\bar{a}$ scattering relates to B(x,z)-symmetry excitations, which involve ionic motion in a plane perpendicular to the polar axis. Brillouin scattering spectra observed in the above two scattering geometries at 410 °C is shown in the inset of Fig. 2. In $a(b,b)\bar{a}$ scattering geometry, we can see the strong central component. However, in $a(b,c)\bar{a}$ geometry, the strong broad central component disappeared, indicating that the central peak has an A(y) symmetry connected to the dynamic disorder of the Ti ions in the octahedra along the polar b axis of $BaTi_2O_5$. This kind of collective motion of Ti ions may be the origin of ferroelectricity in $BaTi_2O_5$.

The presence of the central peak is direct evidence that a relaxation mechanism takes place in $BaTi_2O_5$ and that the relaxation modes play a key role in the lattice dynamics. Concerning relaxation modes in Brillouin or Raman scatter-

ing, there are different origins, static or dynamic. The most important distinction of the origin of the central peak, whether static or dynamic, is the spectral width. The static origin gives rise to a narrow and temperature-independent central peak, while the dynamic origin results in a relatively broad and temperature-dependent central peak. The finer distinctions among various dynamic mechanisms, such as entropy and phonon density fluctuations, degenerate electronic levels, phasons, ion hopping, precursor clusters, and tunneling, are its temperature, symmetry, and wave vector dependence.[10–16]

Similar central peak features that we observed in $BaTi_2O_5$ have been reported in several classical pure and mixed perovskite compounds, such as $KNbO_3$, $BaTiO_3$, and $KTa_{1-x}Nb_xO_3$ in a Raman scattering study.[16,17] Their central peaks have Lorentzian-type shapes centered at the zero-frequency shift that is indicative of a Debye relaxation. The width of the central peaks is temperature dependent, as predicted by the semiclassical model which was first used to explain the dielectric properties and anomalous of the A_1 [transverse optical (TO)] mode in $BaTiO_3$.[18] Later, it was extended to explain the relaxation modes in some relaxor ferroelectrics.[19,20] In this semiclassical model, the thermally excited B ions tunnel through the top of a barrier between the two sites in the eight-site potential which describes a set of off-center positions for the B ions in every perovskite unit cell. The average relaxation time τ in this set of sites can be written as

$$\tau = \tau_o \exp\left(\frac{\Delta V - kT}{kT_o}\right), \tag{2}$$

where $\Delta V = Vo - E$ is the difference between the height of the barrier and the B-ion zero-point energy. $E = kT$ is the average B-ion energy.

$$kT_o = \hbar/2\pi\sqrt{\alpha/m_b}, \tag{3}$$

is related to the mass m_b of B ions and curvature α of the top of the potential barrier. The quantity τ_o^{-1} is a tunneling "attempt" frequency, and a typical physically plausible value for this quantity is several hundred wave numbers. We have attempted to fit the temperature-dependence behavior of the broad central peak in $BaTi_2O_5$ using Eq. (3) with a physically reasonable attempt frequency $1/\tau_o = 670\ cm^{-1}$. These fitting results are shown as a solid line in Fig. 3. The fitting yields $\Delta V = 821\ cm^{-1}$ and $kT_o = 52\ cm^{-1}$. A main assumption of this tunneling modeling is that, in the case of $BaTi_2O_5$ single crystal, the Ti ion in the oxygen octahedra located at the one of the minima of a double-well potential is thermally excited to just below the top of the potential barrier and tunnels from that level to the another potential minima. Since $T_c = 470\ °C$ is equivalent to the thermal energy of $516\ cm^{-1}$, $\Delta V = 821\ cm^{-1} \sim 909\ °C$ is physically reasonable for a thermally excited relaxation process and consistent with the tunneling model for our Brillouin data in which the thermally excited Ti ions have energies just below the top of the barrier and then tunnel through the barrier. As defined earlier, $kT_o \sim \sqrt{\alpha}$, kT_o determines the curvature center of the barrier. A relatively small value ($kT_o = 52\ cm^{-1}$) implies that the barrier width broadens rapidly below the top of the barrier. Therefore, small changes in the thermal energy of Ti ions give rise to large changes in the size of the barrier width through which it must tunnel. This model explains the strong temperature dependence of the relaxation time observed in the high-temperature phase. As noted in Fig. 3, the relaxation time also shows a rather strong temperature dependence below T_c, but slightly weaker than that above T_c. For ferroelectrics, spontaneous polarization appears just below T_c, so that the double-well potential along the polar axis shows a strong asymmetric line shape. For a $BaTi_2O_5$ single crystal below T_c, the asymmetric line shape of the double-well potential resulting from spontaneous polarization suppresses the temperature dependence behavior of the Ti ions under tunneling.

In conclusion, a relaxation mode was observed in the Raman and Brillouin scattering spectra of ferroelectric $BaTi_2O_5$ single crystals. These central peaks have line shapes of Debye relaxation. The temperature dependence of the relaxation time and integrated intensity of the central peak are consistent with the extended semiclassical tunneling model in which the off-center Ti ion in the octahedra tunnels between two sites of a double-well potential. The ferroelectric phase transition shows, at least near the vicinity of T_c, an order-disorder nature. It seems that the spontaneous polarization mainly resulted from the dynamic disorder of the Ti ions in the octahedra along the polar *b* axis of $BaTi_2O_5$.

This work was supported in part by the 21st Century COE program under the Japanese Ministry of Education, Culture, Sports, Science, and Technology.

[1] F. D. Morrison, D. C. Sinclair, and A. R. West, J. Appl. Phys. **86**, 6355 (1999).
[2] W. O. Statton, J. Chem. Phys. **19**, 33 (1951).
[3] F. W. Harrison, Acta Crystallogr. **9**, 495 (1959).
[4] E. Tillmanns, Acta Crystallogr., Sect. B: Struct. Crystallogr. Cryst. Chem. **30**, 2894 (1974).
[5] Y. Akishige, K. Fukano, and H. Shigematsu, J. Electroceram. **13**, 561 (2004).
[6] Y. Akishige, K. Fukano, and H. Shigematsu, Jpn. J. Appl. Phys., Part 2 **42**, L946 (2003).
[7] T. Kimura, T. Goto, H. Yamane, H. Iwata, T. Kajiwara, and T. Akashi, Acta Crystallogr., Sect. C: Cryst. Struct. Commun. **59**, 128 (2003).
[8] U. Waghmare, M. H. F. Sluiter, T. Kimura, T. Goto, and Y. Kawazoe, Appl. Phys. Lett. **84**, 4917 (2004).
[9] R. A. Cowley, Adv. Phys. **29**, 1 (1980).
[10] P. A. Fleury and K. B. Lyons, Solid State Commun. **32**, 103 (1979).
[11] P. A. Fleury and K. B. Lyons, *Light Scattering Near Phase Transitions*, edited by H. Z. Cummins and A. P. Levanyuk (North–Holland, Amsterdam, 1983).
[12] S. Furusawa, T. Suemoto, and M. Ishigame, Phys. Rev. B **38**, 12600 (1988).
[13] B. Mohammadou, G. E. Kugel, F. Brehat, B. Wyncke, G. Mornier, and P. Simons, J. Phys.: Condens. Matter **3**, 9489 (1991).
[14] T. Shima, M. Kasahara, P. Kaung, and T. Yagi, J. Phys. Soc. Jpn. **65**, 1102 (1996).
[15] Y. Tsujimi, T. Matsui, H. Furuta, and T. Yagi, Phys. Rev. B **59**, 28 (1999).
[16] J. P. Sokoloff, L. L. Chase, and D. Rytz, Phys. Rev. B **38**, 597 (1988).
[17] J. P. Sokoloff, L. L. Chase, and L. A. Boatner, Phys. Rev. B **41**, 2398 (1990).
[18] A. Scalabrin, S. P. S. Porto, H. Vargas, C. A. S. Lima, and L. C. M. Miranda, Solid State Commun. **24**, 291 (1977).
[19] F. M. Jiang and S. Kojima, Phys. Rev. B **62**, 8572 (2000).
[20] I. G. Siny, S. G. Lushnikov, and R. S. Katiyar, Phys. Rev. B **56**, 7962 (1997).

Microheterogeneity and field-cooling effects on $Pb[(Zn_{1/3}Nb_{2/3})_{0.955}Ti_{0.045}]O_3$ single crystals probed by micro-Brillouin scattering

Do Han KIM[1*], Jae-Hyeon KO[2], D. C. FENG[3] and Seiji KOJIMA[1]

[1]*Institute of Materials Science, University of Tsukuba, Tsukuba, Ibaraki 305-8573, Japan*
[2]*Department of Physics, Hallym University, 39 Hallymdaehakgil, Chuncheon, Gangwondo 200-702, Korea*
[3]*Shanghai Institute of Ceramics, Chinese Academy of Science, Shanghai, 200050, China*

Microheterogeneity and field-cooling effects were investigated on $Pb[(Zn_{1/3}Nb_{2/3})_{0.955}Ti_{0.045}]O_3$ (PZN-4.5%PT) single crystals by using a high-resolution micro-Brillouin scattering. The temperature dependence of Brillouin shift showed a typical relaxor behavior with marked softening on approaching the diffuse phase transition, but also revealed a clear microareal variation in a rhombohedral phase below 150 ºC which means a heterogeneity exists over a length scale of at least a few microns in PZN-4.5%PT. These two features seem to correlate with the coexistence of both micronsized domains and irregular nanosized domains, recently confirmed by high-resolution domain studies. This complex domain structure may make each microdomain represent different relaxor behaviors due to its own polar nanoregions and their dynamics. When the crystal was cooled under the electric field along the [001] direction from a cubic phase, two field-induced changes were observed in the Brillouin shift at around 143 ºC and 106 ºC. This observation is in good agreement with the dielectric measurements, meaning a medium-range ordered phase exists between short-range ordered and long-range order phases.

* Corresponding author : dhkim@ims.tsukuba.ac.jp

Microheterogeneity and field-cooling effects on $Pb[(Zn_{1/3}Nb_{2/3})_{0.955}Ti_{0.045}]O_3$ single crystals probed by micro-Brillouin scattering

Do Han Kim[a)]
Institute of Materials Science, University of Tsukuba, Tsukuba, Ibaraki 305-8573, Japan

Jae-Hyeon Ko[b)]
Department of Physics, Hallym University, 39 Hallymdaehakgil, Chuncheon, Gangwondo 200-702, Korea

C. D. Feng
Shanghai Institute of Ceramics, Chinese Academy of Science, Shanghai, 200050, China

Seiji Kojima[c)]
Institute of Materials Science, University of Tsukuba, Tsukuba, Ibaraki 305-8573, Japan

(Received 22 March 2005; accepted 27 June 2005; published online 10 August 2005)

Microheterogeneity and field-cooling effects were investigated on $Pb[(Zn_{1/3}Nb_{2/3})_{0.955}Ti_{0.045}]O_3$ (PZN-4.5%PT) single crystals by using a high-resolution micro-Brillouin scattering. The temperature dependence of Brillouin shift showed a typical relaxor behavior with marked softening on approaching the diffuse phase transition, but also revealed a clear microareal variation in a rhombohedral phase below 150 °C which means a heterogeneity exists over a length scale of at least a few microns in PZN-4.5%PT. These two features seem to correlate with the coexistence of both micronsized domains and irregular nanosized domains, recently confirmed by high-resolution domain studies. This complex domain structure may make each microdomain represent different relaxor behaviors due to its own polar nanoregions and their dynamics. When the crystal was cooled under the electric field along the [001] direction from a cubic phase, two field-induced changes were observed in the Brillouin shift at around 143 °C and 106 °C. This observation is in good agreement with the dielectric measurements, meaning a medium-range ordered phase exists between short-range ordered and long-range order phases. © *2005 American Institute of Physics*.
[DOI: 10.1063/1.2012517]

Lead-based perovskite relaxor ferroelectrics are well-known functional materials for industrial applications such as high-permittivity capacitors, ultrasonic transducers and actuators, etc.[1] Physical properties of relaxor ferroelectrics are closely related to their complex perovskite structures and the existence of polar nanoregions (PNR). The dynamics of PNR causes a diffuse and frequency-dependent broad dielectric maximum, broad distribution of relaxation times and aging behaviors at low temperatures.[2] In spite of many experimental and theoretical efforts on relaxors, such as random-field model,[3] dipolar glass mode,[4] and recent spherical random bond-random field model,[5] understanding of the microscopic origin of their complex behaviors is still not enough up to the present.

Complex perovskite relaxor ferroelectric materials such as $Pb[(Zn_{1/3}Nb_{2/3})_{1-x}Ti_x]O_2$ (PZN-x%PT) and $Pb[(Mg_{1/3}Nb_{2/3})_{1-x}Ti_x]O_3$ (PMN-x%PT) single crystals are excellent candidates for electromechanical applications due to their huge piezoelectric properties. Concerning typical relaxors, $Pb(Zn_{1/3}Nb_{2/3})O_2$ (PZN) and $Pb(Mg_{1/3}Nb_{2/3})O_3$ (PMN) crystals show a diffuse, frequency-dependent broad dielectric peak, broad distribution of relaxation times with divergent leading edge on cooling, and a formation of polar nanoregions below the Burns temperature, T_B, far above the temperature of dielectric maximum, T_m.[6] On the other hand, as the composition of Ti increases, PZN-x%PT and PMN-x%PT exhibit structural phase transitions from cubic to tetragonal or rhombohedral symmetries depending on the composition x.[7,8]

Recently, diffraction studies have clarified that the structures of PZN-x%PT and PMN-x%PT near the MPB are more complicated than our knowledge, and monoclinic and/or orthorhombic symmetries appear with and/or without biasing electric field depending on the composition.[9,10] Moreover, it was brought to light by high-energy x-ray and neutron diffraction studies that the ground state of parent PZN and PZN-x%PT with $x<8\%$ might be pseudo-cubic with an unknown phase "X" accompanied by a rhombohedral distortion limited to the outer surfaces of the crystals.[11,12]

Recently, Brillouin scattering has been performed on PZN and PZN-9%PT near the MPB,[13–15] while there is no systematic investigation on the PZN-4.5%PT crystals of which the composition is located at around the middle between the PZN-9%PT and pure PZN. Brillouin spectra of PZN showed typical relaxor behaviors such as a broad softening of the Brillouin shift of acoustic modes with an increase of phonon damping over a wide temperature range,[16] while PZN-9%PT exhibited clear two-step anomalies in both frequency shift and damping corresponding to two successive phase transitions from cubic to tetragonal and tetragonal to rhombohedral phases.[17] In this paper, we report our study on PZN-4.5%PT by using micro-Brillouin scattering in order to understand the field-cooling effects and spatial variation of elastic properties of this composition.

The PZN-4.5%PT single crystals were grown by the Bridgman method and cut for obtaining pseudo-cubic crystal

[a)]Electronic mail: dhkim@ims.tsukuba.ac.jp
[b)]Electronic mail: hwangko@hallym.ac.kr
[c)]Electronic mail: kojima@bk.tsukuba.ac.jp

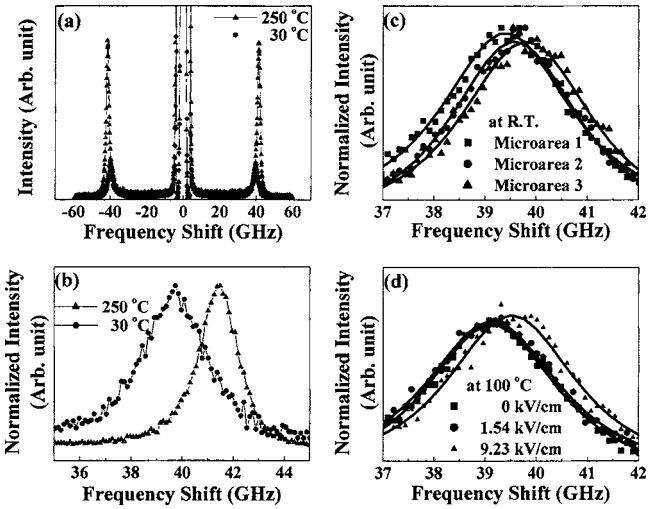

FIG. 1. (a) Brillouin scattering spectra of a PZN-4.5%PT crystal at two temperatures; (b) Brillouin peaks of longitudinal acoustic mode at 250 °C and 30 °C in an extended frequency scale; (c) the microareal dependence of the Brillouin peak at room temperature; (d) the dependence of the Brillouin shift on the biasing electric field at 100 °C. Solid lines in (c) and (d) denote fitting lines.

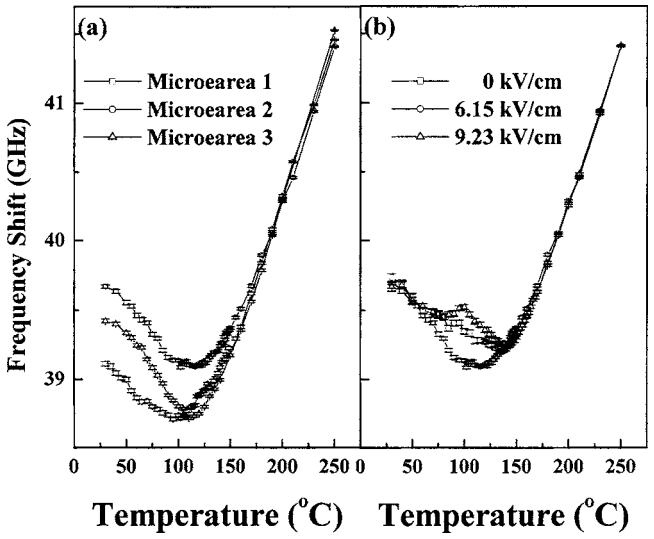

FIG. 2. Temperature dependences of the Brillouin shift of LA mode measured at three different microregions (a) and at three different biasing electric fields on the same microregion (b).

orientations of [100]/[010]/[001]. The crystal dimensions were approximately $6.5\times4.1\times0.65$ mm^3, and the two crystal surfaces perpendicular to the pseudo-cubic [001] direction were polished to the optical grade and coated by ITO. The micro-Brillouin scattering system with a 3+3 pass Sandercock-type tandem Fabry–Perot interferometer (FPI) was used to investigate the elastic properties.[17] A free spectral range and a scan range were 75 and ±60 GHz, respectively. When different microareas were investigated, one micro area was measured and the sample was translated by approximately $100\sim200$ μm by adjusting the X–Y translator. Since we used a backward scattering geometry, both the phonon propagating direction and the biasing electric field direction were along the [001] direction.

Typical Brillouin spectra of the PZN-4.5%PT crystal composed of a longitudinal acoustic (LA) mode and a weak central peak measured at 30 °C and 250 °C are shown in Fig. 1(a). Figure 1(b) shows a clear change of frequency shift and damping factor between 30 °C and 250 °C. Figure 1(c) shows the variation of Brillouin peaks at three different microareas measured at room temperature. Figure 1(d) shows the electric field dependence of the Brillouin peak at the same microareas at 100 °C. As the field increases, the frequency shift moves to higher position in the frequency window. At the field below about 3.0±0.5 kV/cm, Brillouin frequency shift is nearly same as the value measured without any bias field.

The temperature dependences of the Brillouin shift ($\Delta\nu$) measured at three different microareas on the same sample are shown in the Fig. 2(a), where $\Delta\nu$ shows the same value above 200 °C within experimental uncertainty. In contrast, it starts to exhibit slight differences below 200 °C and a relatively large microareal dependence below 150 °C near T_m. As a result, the maximum change of $\Delta\nu$ in microareal dependence at room temperature amounts to approximately 0.6 GHz within the investigated area. This means that rhombohedral phase in the low-temperature range below the diffuse phase transition temperature is characterized by a microheterogeneity. Each microregion probed by micro-Brillouin scattering behaves as if it is an independent relaxor with its own dynamics. This feature cannot be detected by usual macroscopic measurements such as dielectric spectroscopy, since they get the average response from the whole surface of the sample.

In Fig. 2(b), one microregion was chosen for the investigation of field-cooling effects on PZN-4.5%PT using several biasing electric fields. As the electric field increases, Brillouin shift begins to become hardened below approximately 150 °C. In particular, $\Delta\nu$ exhibits a minimum just near 143 °C and a change of slope near 106 °C under the electric field of 6.15 and 9.23 kV/cm. Figure 2(b) points out the field-induced changes in the PZN-4.5%PT crystals at two distinct temperatures. Regarding the temperature dependence of the damping factor (not shown in this paper), it did not show any noticeable changes up to 10 kV/cm within the experimental accuracy.

Figure 3 reveals the microheterogeneity of PZN-4.5%PT in more details. The microregion for the Brillouin measurement was scanned across the surface of the crystal at selected temperatures. The spatial distance between neighboring microregions was approximately $100\sim200$ μm. It is found that

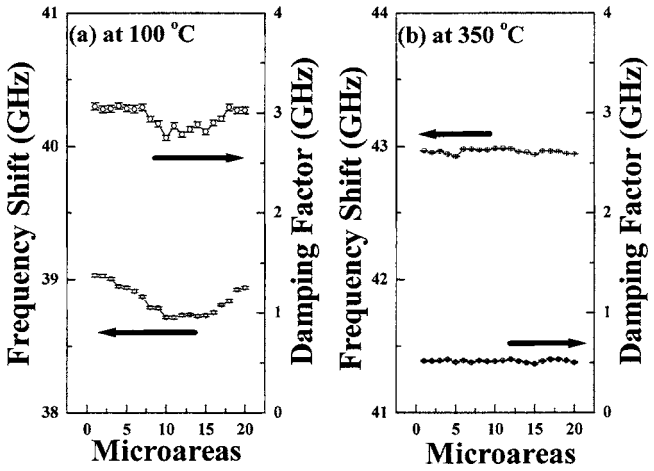

FIG. 3. Microareal dependences of Brillouin shift and damping factor at 100 °C (a) and 350 °C (b).

there is no microareal dependence in $\Delta\nu$ and damping factor in the cubic phase at 350 °C. On the other hand, we can see microheterogeneity clearly in $\Delta\nu$ and damping factor at 100 °C below the diffuse phase transition temperature of 150 °C, consistent with the temperature dependence of $\Delta\nu$ in Fig. 2(a). When we compare these results with those of PZN-9%PT,[18] the Brillouin spectrum itself does not show any noticeable signature for symmetry lowering. This result is in contrast to PZN-9%PT which showed coexistence of several phases such as tetragonal and rhombohedral symmetries depending on what microregion has been chosen.

Our major findings on PZN-4.5%PT single crystals can be summarized as follows: (1) hypersonic frequency $\Delta\nu$ measured without poling field shows typical relaxor behaviors, but it clearly shows a microareal dependence below the diffuse phase transition temperature; (2) two anomalies in $\Delta\nu$ occur at ~143 °C and ~106 °C during field cooling under the bias field of 5~9 kV/cm.

That is, the elastic properties of pure PZN showed a difference between the cooling and heating processes.[14,16] However, PZN-4.5%PT in the present study shows a clear microareal dependence, i.e., the Brillouin shift becomes sensitive to what microregion we choose when the temperature is lower than the diffuse phase transition point. It is noteworthy that this kind of microareal dependence has been reported in the Brillouin studies of other common relaxor single crystals. PMN-35%PT[13] and PZN-9%PT[18] are exceptional because they are located at MPB, which is characterized by quasidegenerate energy states and prone to show different symmetries depending on different microregions. In case of PZN-4.5%PT, each microregion seems to show its own relaxor behavior different from each other near and below the diffuse phase transition temperature. The overall shape of $\Delta\nu$ as a function of temperature is very similar to that of PZN, reflecting relaxor nature of PZN-4.5%PT. Softening of $\Delta\nu$ accompanied by phonon damping over a wide temperature range reveals the order parameter fluctuation owing to the dynamics of PNRs, which is governed by quenched random electric fields and random interactions.

Recent high-resolution domain studies revealed that the domain structure of PZN-4.5%PT is composed of both normal micron-sized domains and irregular nano-sized domains.[19] Irregular domain patterns with the typical sizes 20–100 nm, mainly observed on the (001)-oriented surfaces of unpoled PZN-4.5%PT, was interpreted to be related to the relaxor nature of this composition. It is believed that the coexistence of both the relaxor nature and microheterogeneity from our Brillouin study reflects the complex domain structure in PZN-4.5%PT, where the significant softening in $\Delta\nu$ is related to the dynamics of irregular nanosized domains while the microareal dependence is due to the formation of micronsized ferroelectric domains in which their own irregular nanodomains are incorporated. Therefore, each microdomain represents its own relaxor behavior that is slightly different from one another at low temperatures.

Regarding the field cooling effects in Fig. 2(b), it is worth comparing the present result with previous measurements.[20,21] Figure 2(b) revealed that field-induced successive transitions occur at two critical temperatures around 143 °C and 106 °C. Shen *et al.* observed two anomalies in the dielectric constant under field-cooling and suggested these two anomalies are related to field-induced changes from high-temperature short-range ordered phase to the medium-range ordered phase and then to the long-range ordered ferroelectric state at low temperatures. Two-step changes in the remanent polarization were also observed at the same temperatures. These two critical temperatures correlate well with those of two anomalies in $\Delta\nu$ as can be confirmed from Fig. 2(b). These two temperature ranges are also in good agreement with the phase diagram suggested by Lu *et al.*[21] Shen *et al.* reported that a small bias field of 0.65 kV/cm was enough for inducing the above two phase transitions, since the direction of the electric field was along the polar direction [111] of the rhombohedral phase. In our study, the biasing field was applied along the [001] direction, and an electric field one order of magnitude higher than 0.65 kV/cm was necessary to induce two clear anomalies in the acoustic properties of PZN-4.5%PT crystal.

In summary, Brillouin spectrum of PZN-4.5%PT showed both a typical relaxor behavior and a microheterogeneity. This was ascribed to the coexistence of micron-sized domains and irregular nano-sized domains.[19] This complex domain structure may make each microdomain, which begins to form near the diffuse phase transition temperature at ~150 °C, experiences its own freezing dynamics owing to the interactions of PNRs in the environment of quenched random fields and complex domain configurations in which orthorhombic, monoclinic, or even triclinic symmetry might be expected.[22] Two anomalies were induced at ~143 °C and ~106 °C under the poling field along [001]. These two temperatures are in good agreement with previous dielectric studies and seem to indicate the medium-range ordered state between the high-temperature short-range and low-temperature long-range ordered phases.[20]

[1] K. Uchino, *Ferroelecric Devices* (Marcel Dekker, New York, 1999).
[2] L. E. Cross, Ferroelectrics **76**, 241 (1987).
[3] V. Westphal, W. Kleemann, and M. D. Glinchuk, Phys. Rev. Lett. **68**, 847 (1992).
[4] D. Viehland, S. J. Jang, L. E. Cross, and M. Wuttig, J. Appl. Phys. **68**, 2916 (1990).
[5] R. Pirc and R. Blinc, Phys. Rev. B **60**, 13470 (1999).
[6] D. La-Orauttapong, J. Toulouse, J. L. Robertson, and Z.-G. Ye, Phys. Rev. B **64**, 212101 (2001).
[7] S. Nomura, T. Takahashi, and Y. Yokomizo, J. Phys. Soc. Jpn. **27**, 262 (1969).
[8] J. Kuwata, K. Uchino, and S. Nomura, Jpn. J. Appl. Phys., Part 1 **21**, 1298 (1982).
[9] G. Xu, H. Hiraka, and G. Shirane, and K. Ohwada, Appl. Phys. Lett. **84**, 3975 (2004).
[10] G. Xu, D. Viehland, J. F. Li, P. M. Gehring, and G. Shirane, Phys. Rev. B **68**, 212410 (2003).
[11] G. Xu, Z. Zhong, Y. Bing, Z.-G. Ye, C. Stock, and G. Shirane, Phys. Rev. B **67**, 104102 (2003).
[12] K. Ohwada, K. Hirota, P. W. Rehrig, Y. Fujii, and G. Shirane, Phys. Rev. B **67**, 094111 (2003).
[13] F. M. Jiang and S. Kojima, Appl. Phys. Lett. **77**, 1271 (2000).
[14] Y. Gorouya, Y. Tsujimi, M. Iwata, and T. Yagi, Appl. Phys. Lett. **83**, 1358 (2003).
[15] J.-H. Ko, D. H. Kim, and S. Kojima, Appl. Phys. Lett. **83**, 2037 (2003).
[16] M. H. Kuok, S. C. Ng, H. J. Fan, M. Iwata, and Y. Ishibashi, Appl. Phys. Lett. **78**, 1727 (2001).
[17] D. H. Kim, S. Kojima, and J.-H. Ko, J. Korean Phys. Soc. **46**, 131 (2005).
[18] F. M. Jiang and S. Kojima, Ferroelectrics **266**, 19 (2002).
[19] I. K. Bdikin, V. V. Shvartsman, and A. L. Kholkin, Appl. Phys. Lett. **83**, 4232 (2003).
[20] M. Shen, J. Han, and W. Cao, Appl. Phys. Lett. **83**, 731 (2003).
[21] Y. Lu, D.-Y. Jeong, Z.-Y. Cheng, T. Shrout, and Q. M. Zhang, Appl. Phys. Lett. **80**, 1918 (2002).
[22] J. Yin and W. Cao, J. Appl. Phys. **92**, 444 (2002).

Vibrational spectrum of Hen Egg White Lysozyme

Anna SVANIDZE

A.F. Ioffe Physical Technical Institute of RAS, Saint-Petersburg, Russia

The dynamics of globular proteins is of prime importance to the understanding of their functions. It is especially important to investigate low frequency vibrations in proteins, which presumably reveal collective motions involving a large part of the macromolecule.

As pointed out in papers [1], the features of the vibrational dynamics in proteins are related to the fact that their structure and properties may well described in the framework of fractal approach. The fractality of proteins suggests that a fracton excitation in their vibrational spectrum should exist, and it can be identified by analysis of density of states (DOS) of protein. According to work Granek and Klafter [2] computer simulations have shown that $\tilde{d}$ varies from one protein to another covering the range $1.3 < \tilde{d} < 1.9$, but there not exist experimental investigation of fracton behavior in proteins. So the main purpose of our work is to identify and distinguish phonon and fracton contributions into the low frequency dynamics of hen egg white lysozyme (HEWL).

Thus we have determined and analyzed the generalized density of states of HEWL using the results of inelastic incoherent neutron scattering. Inelastic neutron scattering was measured by a KDSOG-M inverse-geometry time-of-flight spectrometer placed at the 10^{th} channel of a pulsed high-flux IBR-2 reactor (FLNP, JINR, Dubna) at temperatures 200K, 280K, and 311K. As a result of our experiments, we were succeeded in distinguishing the phonon and fracton regimes in the low-frequency part of the DOS of HEWL and characterizing these excitations by corresponding spectral dimensions at mentioned temperatures. Not great temperature dependences of both spectral dimensions are also revealed [3].

References

[1]. J.S. Helman et al, Phys. Rev. Lett., **53** (1984) 195; Turkan Haliloglu et al, Phys. Rev. Lett., **79** (1997) 3090; M.Nollmann and P.Etchegoin, Phys.Rev. E, **60** (1999) 4593; M. B. Enright and D. M. Leitner, Phys. Rev. E, **71** (2005) 011912; H.J. Stapleton et al, Phys. Rev. Lett., **45** (1980) 1456; Daniel ben-Avraham, Phys. Rev. B, **47** (1993) 14559;

[2]. R. Granek and J. Klafter, Phys. Rev. Lett., **95** (2005) 098106;

[3]. S.G. Lushnikov et al, JETP Letters, Vol. **82** (2005) 30–33.

Organized by
Institute of Materials Science, University of Tsukuba